

SLAC-168
(T/E)
UC-34d

MULTIPLICITIES AND REGGE POLES IN DEEP
HADRON-HADRON SCATTERING*

ROBERT STEVEN SAVIT

STANFORD LINEAR ACCELERATOR CENTER

STANFORD UNIVERSITY

Stanford, California 94305

PREPARED FOR THE U. S. ATOMIC ENERGY
COMMISSION UNDER CONTRACT NO. AT(04-3)-515

December 1973

Printed in the United States of America. Available from National Technical Service, U.S. Department of Commerce, 5285 Port Royal Road, Springfield Virginia 22151. Price: Printed Copy \$5.45.

* Ph. D. dissertation.

ABSTRACT

We discuss some aspects of hadron-hadron scattering in the deep region. The deep region can be very roughly characterized as the kinematic region which involves large momentum transfers at high energies. Using ideas related to Feynman's parton model, we derive a formula for the average multiplicity of an inclusive or semi-inclusive experiment in which at least one final-state particle is detected with a large transverse momentum, and we show how the average multiplicities in these experiments are related to average multiplicities in other high energy reactions. We then turn to a discussion of the relationship between the deep and Regge regions in $2 \rightarrow 2$ hadronic amplitudes. An integral equation, based on t -channel iterations of two-particle irreducible kernels is derived. We show how these graphs generate Regge poles and how their trajectories are connected to the deep scattering Born term. Physical implications of our procedure are then discussed. Next, we generalize our approach to include coupled channel problems. We then show how to include the effects of signature in the scheme, and we end with some speculations about the physical interpretation of Harari-Rosner duality diagrams and the dynamical origin of the Pomeron pole.

If I make a mark in time
I cannot say the mark is mine.

Cat Stevens

ACKNOWLEDGMENTS

For three years I have had the privilege of knowing and learning from Professor Richard Blankenbecler. To him go my warmest thanks. The informal hospitality of his office, as well as his professional inspiration and personal encouragement are deeply appreciated and will not be forgotten.

Many other people have also contributed in various ways to my graduate education. While at SLAC, I have been fortunate in learning from and/or working with Yoram Avni, Stanley J. Brodsky, James D. Bjorken, Martin B. Einhorn and T. Neff, among others. It is a pleasure to thank all these people. My friend, Joseph Kiskis is acknowledged in a separate sentence because his contributions include, but go far beyond physics. Thank you, Joe.

Sidney D. Drell has in many direct and indirect ways helped to make my time at SLAC profitable and enjoyable, and I am grateful to him for that. I also want to thank Sharon Jensen for her friendliness and help during the past three years.

There are, of course, others to whom I owe much, but it is not the custom to thank them here.

TABLE OF CONTENTS

	Page
I. INTRODUCTION	1
II. MULTIPLICITIES IN DEEP HADRON-HADRON SCATTERING . .	3
III. REGGE POLES IN DEEP HADRON-HADRON SCATTERING . .	23
A. Introduction	23
B. The Basic Integral Equation	24
C. The Coupled Channel Case	80
D. Signature, Duality Diagrams and the Pomeron	97
IV. SUMMARY AND CONCLUSIONS	117

LIST OF FIGURES

	<i>Page</i>
1. Parton distribution immediately after an ordinary hadron-hadron collision.	5
2. Final, average distribution of hadrons after an ordinary hadron-hadron collision.	7
3. Parton distribution immediately after a deep inelastic lepton-hadron collision.	11
4. Final distribution of hadrons after a deep inelastic lepton-hadron collision.	13
5. Parton distribution immediately after deep hadron-hadron scattering.	14
6. Final, average hadron distribution associated with deep hadron-hadron scattering events.	16
7. Sample Feynman diagram for illustration of old-fashioned perturbation theory in the infinite momentum frame.	26
8. One of 20 time orderings of Fig. 7 that vanish in the infinite momentum frame.	30
9. Time orderings of Fig. 7 that survive in the infinite momentum frame.	31
10. Graphical illustration of amplitude, \mathcal{M}_j	34
11. The recursion relation connecting \mathcal{M}_{j+1} with \mathcal{M}_j	35
12. The recursion relation in terms of integrals over the spectral functions of the subamplitudes.	42
13. The full integral equation.	44
14. Simple ladder graph.	60

	Page
15. (tu) parton interchange diagram.	62
16. Feynman diagram showing kernel which includes a vertex correction.	63
17. Feynman diagram showing kernel which has a non-zero third double spectral function. (su- spectral function.)	64
18. Time orderings which contribute to the Feynman diagram Fig. 16 in the infinite momentum frame. The dashed lines show which intermediate state particles are on their mass shells.	66
19. Contributions to Fig. 17. The intermediate state particles that are on mass-shell are indicated by the dashed lines.	72
20. Possible contributions to the imaginary part of the Feynman diagram, Fig. 17. Figure 20 a does not contribute for stable external particles.	73
21. Only surviving time ordering for the old-fashioned perturbation theory calculation of simple ladder graphs.	75
22. Some examples of the Harari-Rosner duality diagrams.	98
23. (st) parton-interchange graph.	104
24. (su) parton-interchange graph.	105
25. Simple amplitudes with (a) u-channel and (b) s-channel singularities (in this case poles).	108
26. Feynman diagrams resulting from the convolution of sub- amplitudes as in Fig. 25; (a) is the result of $u \times u$ and (b) is the result of $s \times u$	109

CHAPTER I

INTRODUCTION

One of the most prominent and general features of high energy hadron-hadron scattering is the fact that the transverse momenta of the final state particles are severely limited. This observation applies both to elastic and inelastic reactions, and holds with only minor modifications over a large range of energies. For example, a hadron-hadron elastic cross section is typically five to ten orders of magnitude smaller at $|t| \sim 1 \text{ GeV}$ than it is at $|t| = 0$.

This kinematic region (high s , small $|t|$) may be called the Regge region since hadronic events populating this region are often described by the exchange of Regge trajectories which correspond to singularities in the complex angular momentum plane. From a field-theoretic point of view, the origin of these singularities is not clear, but the common wisdom is that the trajectories which dominate the Regge region arise from "coherent" effects in which many different T-products must be added together to produce Regge behavior. The simplest example of this is summing the infinite set of ordinary ladder graphs in, say, ϕ^3 -theory to produce a moving Regge pole.

While most hadronic events occupy the Regge region, an important few lie outside this domain. They are important because unlike the Regge dominated events, these deep events presumably do not require coherent contributions from many Feynman graphs. This region is called the deep region because the large momentum transfers involved probe small distances or impact parameters, and allow us to see more of the detailed structure of the hadrons. Of course, all these words are reminiscent of statements made about inelastic lepton-hadron scattering in the Bjorken limit, and indeed, many of the intuitions developed by physicists for that process can be applied to deep hadron-hadron scattering.

In this work, we want to investigate some aspects of the deep region in hadron-hadron scattering. We shall treat two rather different problems. In Chapter II, we derive a formula for the average multiplicity in an inclusive or semi-inclusive experiment in which at least one final-state hadron is detected with a large transverse momentum. The basis of the derivation is a parton model with direct parton-parton scattering, although the final result may well be more general. In Chapter III we turn to exclusive hadronic reactions — in particular, $2 \rightarrow 2$ amplitudes — and discuss how the deep region is related to the Regge region. After a brief introduction (section III.A), we derive and examine an integral equation which Reggeizes deep scattering. This equation is based on t-channel iterations of an irreducible kernel and can be used to see how deep scattering joins smoothly onto the Regge region. Furthermore, the role played by coherence effects in near forward scattering are especially clear in this approach. All this is done in section III.B. In section III.C, we generalize the equation derived in section III.B to include coupled channel problems in which more than one kind of hadron is allowed to participate in the scattering amplitudes. We show that in order to preserve the factorization property of Regge pole residues we must, in general, introduce extra poles into the description of the amplitudes, the number of poles being proportional to the dimensionality of the relevant channel space. Chapter III ends with section III.D in which, after quick reviews of duality diagrams and the parton-interchange theory of deep scattering, we show how to include signature in our Reggeization scheme. We then proceed to discuss the relationship between duality diagrams and parton-interchange diagrams, as well as some ideas and speculations about the origin of the Pomeron pole. Finally, in Chapter IV, we present some conclusions along with a summary of what we have learned.

CHAPTER II

MULTIPLICITIES IN DEEP HADRON-HADRON SCATTERING

The ultimate goal of this section is to derive a formula which describes the average number of particles produced in a high-energy hadron-hadron collision when at least one particle is observed with a large transverse momentum. Our discussion will be based largely on ideas of the Feynman parton model and we shall draw heavily on the work which others have done in elaborating and applying these ideas. As we go along, the reader may well feel some discomfort at the evident lack of rigour in our arguments. We therefore offer our apologies now and disclaim any responsibility for the tearing of hair and the rending of garments which may result from one's participation in these pages. Those with weak hearts are advised to skip to Chapter III where they may rest peacefully in the bosom of mathematical formulae.

Let us begin, then, with a review of some ideas about multiplicities in various high energy processes. Specifically, we will need to discuss multiplicities in ordinary hadron-hadron scattering, $e^+ - e^-$ annihilation, and deep inelastic lepton-production. This is necessary because our formula for deep h-h (h is a hadron) multiplicities involves terms related to these other processes. Let us first turn to ordinary h-h multiplicities.

It is a well-established phenomenological observation that in high energy h-h collisions final state particles generally have limited transverse momenta.^{1,2} That is, the great majority of events in h-h interactions yield particles with $|p_{\perp}| \lesssim \frac{1}{2}$ GeV. By ordinary h-h events, we mean just these events. Of course, the cutoff at $\sim \frac{1}{2}$ GeV is approximate only — say within a factor of two — and, in any case, may not be entirely energy independent. At the present time we do not wish to take a firm stand on the exact condition which distinguishes the

ordinary from the deep scattering regions. This will be discussed more fully in Chapter III (p. 57). For the time being, however, it will be sufficient to rely on the vague condition given above. We also note that since events which have a particle with large $|p_{\perp}|$ are so rare, it is probably not necessary from an experimental point of view to distinguish between the average multiplicity of ordinary h-h events, and the average multiplicity of all h-h collisions for a given pair of initial state particles.

The result we seek for ordinary h-h scattering can be obtained from many different sets of assumptions;¹ however, to put the reader in the right frame of mind, we shall approach it from Feynman's point of view.^{3,4,5} Consider a h-h collision in the center of mass with the hadrons moving along the z-axis. At high energies, the hadron, which is an extended object, or rather, has a field (or fields) associated with it which have spatial extent, gets Lorentz contracted along its direction of motion. As $s \rightarrow \infty$, the distribution of field energy in z becomes a δ -function. Since the Fourier transform of a δ -function is a constant, we are led to expect a constant density of energy per unit interval in p_z . Thus, the density of field quanta must be $\propto dp_z/E$. Now, since p_{\perp} is limited for the final state particles in a h-h collision, we make the assumption that it is limited for the field quanta or constituents also. This is reasonable if one remembers that the Lorentz contraction takes place only in the direction of motion, so the transverse degrees of freedom are unaffected. If we plot the distribution of constituents in momentum space for the two colliding hadrons, we get a picture like that of Fig. (1). The horizontal axis, instead of p_z is rapidity defined as $y = \frac{1}{2} \ln[(E + p_z)/(E - p_z)]$. The distribution for each hadron is flat in rapidity except near $x = 0, \pm 1$, where $x \equiv 2p_z/\sqrt{s}$. We may therefore picture a fast

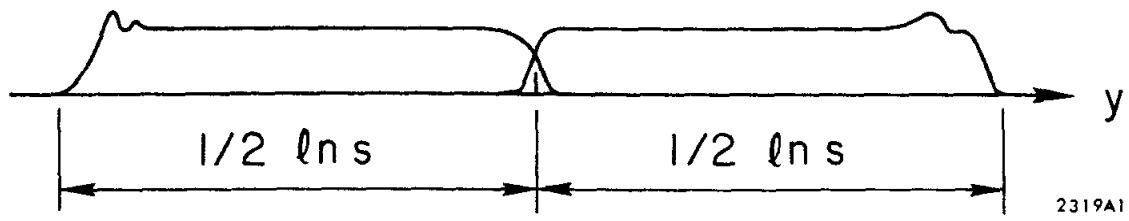


FIG. 1--Parton distribution immediately after an ordinary hadron-hadron collision.

moving hadron as a bag of field quanta, i , moving mostly in the same direction, and distributed more or less as dE_i/E_i .

The next step in the scattering process is described by saying that the constituents from the two hadrons — called partons by Feynman — which are near $x = 0$ interact with each other to smooth out the final parton distribution so it looks like Fig. (2). The hadrons interact through these "wee" partons, according to Feynman, either by direct scattering, or perhaps, predominately by parton exchange. Since the wee partons have small p_z it is very easy for them to get confused and forget to which hadron they belong. This mixing up of wee constituents is the mechanism by which most hadronic reactions are supposed to take place. It is, of course, much more difficult for a very energetic parton from one hadron to get confused, since that would require a large change in its momentum. Another way of saying this is to say that only partons which are relatively close to each other in momentum space can directly interact. An energetic parton, therefore, has only second-hand information about the hadron to which it does not belong — it must wait for information to reach it by a series of close neighbor interactions.

All of this, of course, sounds a lot like the behavior one might expect from a gas contained in an almost one dimensional cylinder.⁶ In these terms, one says that the wee partons interact and come to equilibrium with the rest of the gas. But another, perhaps more convincing way of understanding why the parton density is uniform in rapidity, is that there is apparently no reason why we needed to choose the center of mass to formulate the original idea. Another frame boosted by an amount $p_z = x(\sqrt{s}/2)$, where x is some finite fraction would work just as well. Therefore, there is nothing to single out the center of mass frame, and even if the parton densities in the incident hadrons were different

■ Fragmentation Regions

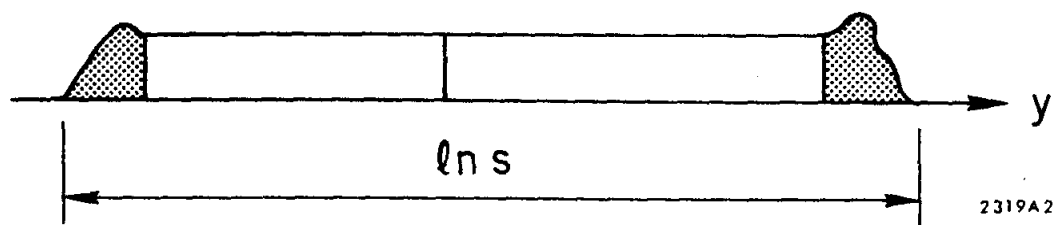


FIG. 2--Final, average distribution of hadrons after an ordinary hadron-hadron collision.

to begin with, after the interaction they must be the same. Of course, at $x = \pm 1$ the distributions must go to zero by energy conservation, and these arguments do not shed any light on the behavior of the distributions in these hadron fragmentation regions.

Before we can hope to relate these parton ideas to the description of h-h scattering, we need a mechanism for turning the partons into hadrons. Since, as we shall see below, partons have been endowed by their creator with certain (perhaps inalienable) point-like form factors, the partons, according to the orthodox view, cannot be ordinary hadrons. (Frankly, I don't believe this.) Fortunately, we do not need a specific mechanism to get the result we seek. We only need to make the probably plausible assumption that the final hadron distribution is proportional to final parton distribution. With this assumption, we find from Fig. (2) the well-known asymptotic multiplicity formula for h-h scattering

$$\langle n \rangle_h = C_h \ln s; \quad s \rightarrow \infty \quad (2.1)$$

where C_h measures the density of hadrons in the hadron plateau.

Let us now take these ideas and try to apply them to e^+e^- annihilation processes. As long as one is proposing the idea that hadrons are made up of some kind of constituents, one may as well assume that the constituents are point-like (in some sense) in order to explain the SLAC-MIT deep inelastic electroproduction experiments. The standard parton description for e^+e^- annihilation can then be stated as follows:^{4,5,7} we assume that only processes which are lowest order in α contribute. The electron-positron pair, therefore, annihilate into one time-like photon of mass Q^2 which in turn decays into a parton-antiparton pair. As in the case of hadrons, we may think of the wave function of the spat

out parton getting contracted along its direction of motion. Arguments analogous to the ones presented above for the case of h-h scattering will then give a similar picture for the final hadron distribution in e^+e^- annihilation. With the replacement $s \rightarrow Q^2$, we may view Fig. (2) as the average final hadron distribution for the annihilation experiment. Of course, in this case the fragmentation regions near $x = \pm 1$ are parton fragmentation regions, not hadron fragmentation regions. The asymptotic multiplicity formula for e^+e^- annihilation is therefore

$$\langle n \rangle_{e^+e^-} = C_{e^+e^-} \ln Q^2; \quad Q^2 \rightarrow \infty. \quad (2.2)$$

We remark in passing that another way to understand the final hadron distribution in this experiment is to say that the parton and antiparton each bremsstrahlung particles, which fill up the rapidity gap between them. The distribution is smoothed out by the interactions of each particle with its near neighbors.

Before turning to deep h-h scattering we need to briefly discuss the multiplicities expected in deep inelastic lepto-production for large ν and Q^2 . The parton model for this process^{5, 7, 8, 9, 10} pictures the virtual γ (for electro-production) or W (for neutrino-production) knocking a parton out of the target hadron. For our purposes, it is convenient to analyze the situation in the Breit frame of the struck parton.⁸ In this frame we have a collection of partons moving to the right and a space-like photon or W moving to the left. One of the partons is struck by the photon absorbing its momentum and thereby reversing the direction of its own momentum. In this frame the z -component of the initial momentum of the struck parton is $p_z = x(M\nu / \sqrt{Q^2}) = \sqrt{Q^2}/2$, where $Q^2 = -q_\mu q^\mu$ and $M\nu = p_\mu q^\mu$, q_μ being the photon's (W 's) four-momentum and p_μ being the hadron's initial four-momentum.

The distribution of partons in momentum space immediately after the interaction is shown in Fig. (3). On the left we have an isolated parton which, by arguments similar to those presented above for e^+e^- annihilation, we expect to cascade into a final parton distribution which is uniform in rapidity, and when it finally turns into hadrons has a density $\propto C_{e^+e^-}$. On the right we have the remnants of the target hadron. Notice in particular (i) the hole in the distribution created by the absence of the struck parton,¹¹ and (ii) the fact that the parton distribution goes to zero at $y = \ln[(\omega - 1)\sqrt{Q^2}]$, where $\omega \equiv 1/x$. This is required by energy conservation since after the removal of the parton the energy left in the hadron is $\sim (\omega - 1)\sqrt{Q^2}$ and the presence of a parton with energy greater than this would violate energy conservation. Notice also that we cannot consider the hole to be the presence of a negative energy antiparton, since if partons are fermions, the negative energy sea is filled, and if they are bosons, it is not clear how to apply this idea.

Now, as we said before, we expect a parton plateau to develop from the isolated parton. The wee partons from this cascade will mix with the wee partons from the remainder of the target and, as in other such cases, will smooth out the parton distribution in the region of the origin. Upon reflection, we see that we could have performed this analysis in a number of other frames with origins anywhere between the hole and the final position of the struck parton. This means that the parton distribution cannot depend on the choice of frame and so must be uniform in rapidity in this region. Because of the implicit assumption of short range correlations, we do not expect the distribution of partons to the right of the hole to be significantly affected by all this, so the parton plateau there should stay pretty much the same.

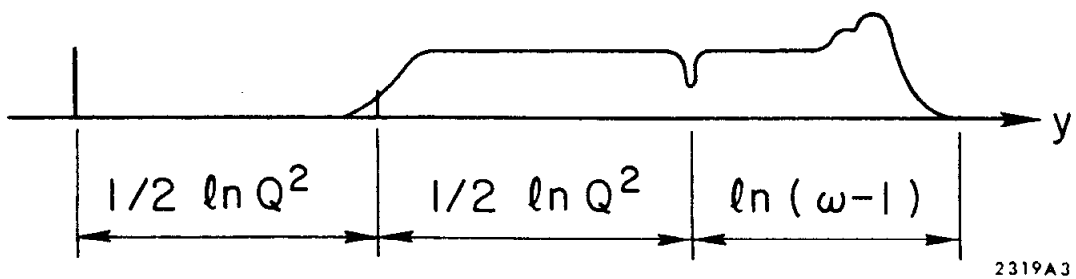


FIG. 3--Parton distribution immediately after a deep inelastic lepton-hadron collision.

The final parton distribution, therefore, is shown in Fig. (4). In addition to the two plateaus (which will give hadron plateaus of heights $C_{e^+e^-}$ and C_h), there are three fragmentation regions (parton, hole and target) which stay finite as $\nu, Q^2 \rightarrow \infty$. Assuming that the final hadron distribution resembles this parton distribution, the average multiplicity for large ω and Q^2 will be given by

$$\langle n \rangle_{lh} = C_{e^+e^-} \ln Q^2 + C_h \ln(\omega-1) . \quad (2.3)$$

Having finished our review of the Feynman parton model and some of its previous applications, we now turn to the main task of this section: deriving a multiplicity formula for deep hadron-hadron scattering.¹² In what follows, we shall refer to the notion of direct parton-parton scattering. However, we do not believe that our results depend crucially on the nature or existence of such an interaction. The hard parton-parton scattering is used here merely as a device for producing partons with large transverse momenta. While this approach seems close in spirit to that of Berman, Bjorken and Kogut,⁹ our results may also be consistent with a parton interchange theory such as that of Gunion, Brodsky and Blankenbecler¹³ in which direct parton-parton scattering does not play a role.

With these remarks in mind, let us begin by considering the inclusive process $a + b \rightarrow c + X$ where c has a large transverse momentum, $p_{\perp c}$. In the following, we shall always work in the center-of-mass of a and b , unless we specify otherwise. The picture we have in mind for the production of particles with large p_{\perp} involves two stages. First, a high energy parton from a scatters off a high energy parton from b , both receiving a large sideways kick. The parton distribution in phase space immediately after the scattering is shown in Fig. (5).

■ Fragmentation Regions

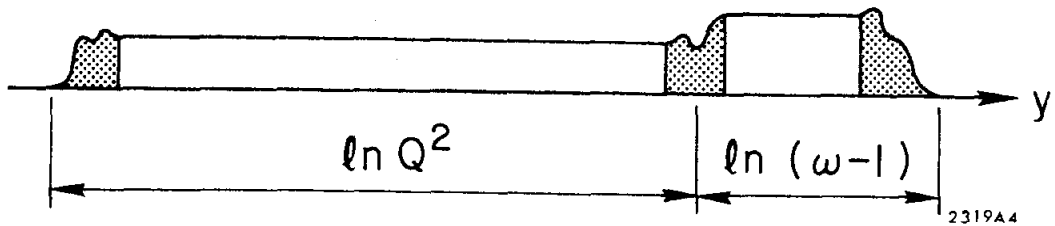
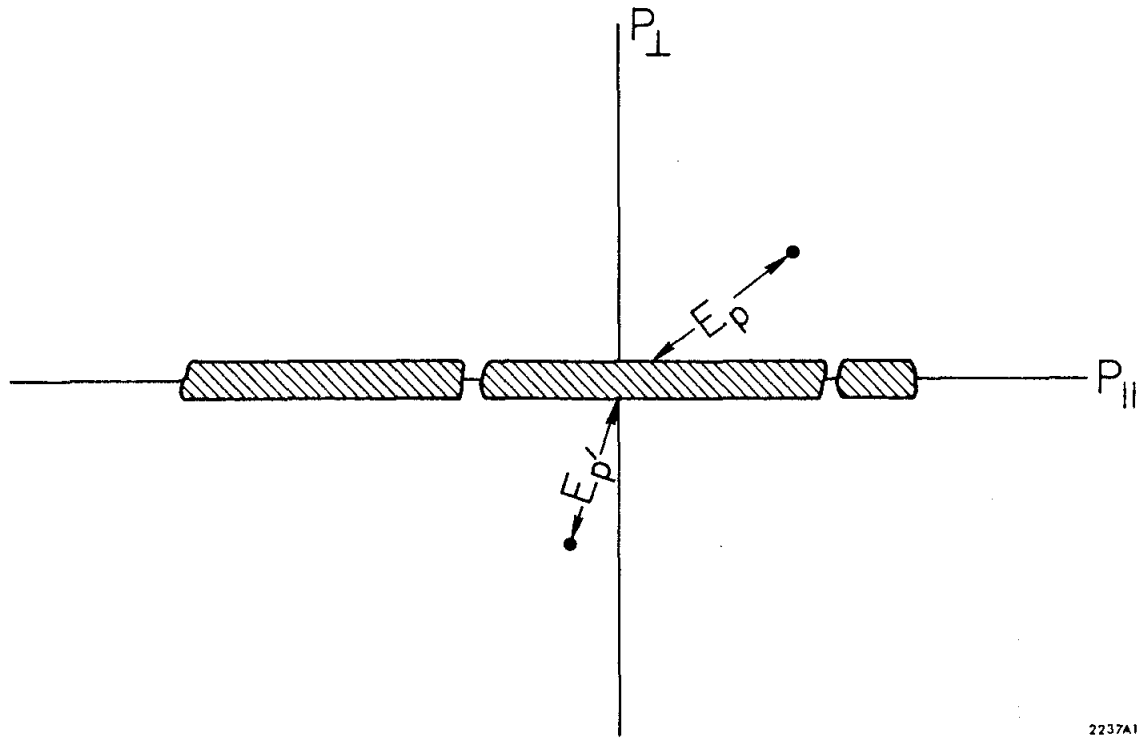


FIG. 4--Final distribution of hadrons after a deep inelastic lepton-hadron collision.

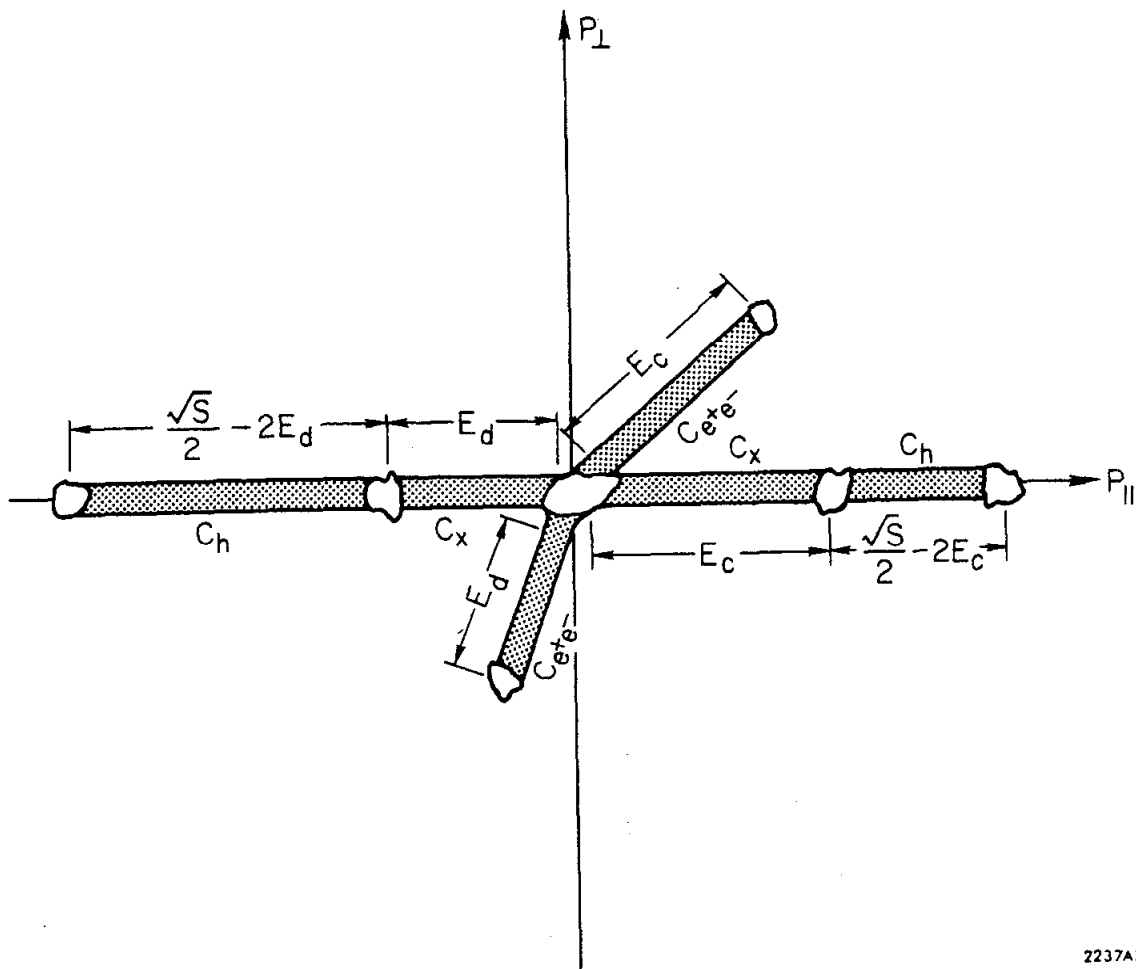


2237A1

FIG. 5--Parton distribution immediately after deep hadron-hadron scattering.

Next, the two partons which are each isolated in phase space separately evolve into hadrons in a way which is more or less independent of each other, as well as independent of the remaining pieces of a and b . At sufficiently high energies and momentum transfers, we expect that each such isolated parton will contribute $\sim C_{e^+e^-} \ln E_p$ to $\langle n \rangle$ for this reaction. E_p is the parton's energy in the $a+b$ center of mass. This result follows from the observation that these partons are isolated in phase space, and should produce final state particles just as the isolated partons in e^+e^- annihilation do. That is, we will have hadrons distributed, on the average, as dE/E in a cylinder in phase space pointing in the direction of the liberated parton plus, perhaps, a finite parton fragmentation region. A possible exception to this is when the parton-parton scattering angle is small in the parton-parton center of mass.¹⁴ (See below for a discussion of this point.) These regions are shown in Fig. (6) where we display the average final hadron distribution for our deep scattering event.

In addition to the e^+e^- plateaus developed by the isolated partons, the remaining pieces of a and b develop certain plateaus and fragmentation regions. Furthest from the origin we have the fragmentation regions of a and b . Moving in along the p_{\parallel} axis, we next encounter two plateau regions. Here we also expect a distribution of hadrons like dE/E , but the coefficient in this case is C_h . Next, we have the hole fragmentation regions which result when the remaining partons try to heal the wound left in a and b by the removal of the two partons. Notice that these configurations (hadron fragmentation region, hadron plateau, hole fragment region) are exactly what appear in part of the lepto-production distributions (Fig. 4). Finally, we have two more plateaus of density C_x , as yet unknown (we shall return to this point later), and a finite overlap region at the origin where the tails of all the final hadron distributions come together.



2237A2

FIG. 6--Final, average hadron distribution associated with deep hadron-hadron scattering events.

At sufficiently large s and $p_{\perp c}$, the major contribution to the average multiplicity of the reaction $a + b \rightarrow c + X$ comes from the six plateau regions, and is given by

$$\langle n(s, p_{\perp c}, E_c) \rangle_{\text{deep}} = (C_{e^+e^-} + C_X) \ln E_c^2 + \theta(s - 16E_c^2) C_h \ln \left(\frac{\sqrt{s}}{2E_c} - 1 \right)^2. \quad (2.4)$$

Notice that the right-hand side depends on $p_{\perp c}$ only through E_c . E_c is the energy of c in the $a+b$ center of mass, and the θ function is included so that the term $\propto C_h$ will not contribute when $4E_c \geq \sqrt{s}$. This, of course, is required by energy conservation. We have neglected terms which stay finite as $s, p_{\perp c} \rightarrow \infty$. These correction terms include the contribution to the multiplicity from the finite fragmentation and overlap regions, as well as certain factors which multiply the arguments of the logs. Some of these factors come from averaging over the possible orientations of the undetected parton cylinder, and depend in detail on the parton-parton scattering amplitude and the parton distributions in a and b . The others arise when we write E_p in terms of E_c , since $E_c = f_p E_p$, where f_p is some finite fraction. However, none of these complications change the asymptotic formula (2.4).

This formula has several interesting features. When $E_c \sim \langle m_{\perp} \rangle$ (say, about 1 GeV), Eq. (2.4) gives $\langle n \rangle \sim C_h \ln s$, and we recover the well-known expression for the multiplicity in ordinary hadron-hadron scattering. On the other hand, when E_c^2 is some finite fraction of s , and the scattering angle is greater than zero, we find $\langle n \rangle \sim (C_{e^+e^-} + C_X) \ln E_c^2$, and the multiplicity becomes essentially independent of the second term. Of course, if the scattered partons have essentially all of the incident hadrons' energy, there is no plateau along p_{\parallel} and the term $\propto C_X$ is absent.

There are two somewhat technical aspects of Eq. (2.4) and its derivation we would now like to discuss. First, as implied above, we note that if we detect a hadron with a large p_{\perp} , we can be fairly certain that it is the most energetic hadron in its cylinder, and therefore has some fixed, finite fraction of its parent parton's energy. The reason is that the probability of knocking a parton to a distant region of phase space falls rapidly with the parton's energy. So, if we observe a widely scattered hadron with energy $E_c \gg \langle m_{\perp} \rangle$, it is unlikely that another hadron with energy $> E_c$ was produced by the same parton since the parton's energy would then have had to have been extremely large. We can make this argument somewhat more quantitative as follows: suppose the probability to produce a parton at large $p_{\perp} \propto E_p^{-N}$, where N is some fairly large number. On the average the k th hadron produced in the parton cylinder will have energy $f_p^k E_p = E_h$, where $C_{e^+e^-} \ln f_p = -1$. If we observe an energetic hadron with energy E_h , the probability that it is the k th hadron produced by a parton $\propto f_p^{kN} / E_h^N$. Therefore, if $f_p^N \ll 1$, we can be fairly certain that the hadron we observe is the most energetic in the parton's cylinder.

Second, we note that the derivation of Eq. (2.4) is based on an average over configurations of final hadrons as pictured in Fig. (6). Let us now ask what specific dynamical mechanisms for the production of hadrons by isolated partons are consistent with this picture. We may roughly characterize various mechanisms in terms of how the isolated partons finally communicate with the rest of the scattering system. One possibility, which is obviously consistent with Fig. (6) is that the isolated partons form cylinders of hadrons to communicate with the wee partons in the center of mass of $a + b$. However, there are at least two other very plausible possibilities: (1) in the center of mass of the two scattered partons, a straight cylinder joining the partons may develop, or

(2) in the rest frame of the hole (i.e., the rest frame of the scattered parton before it was scattered), a straight cylinder may develop between the hole and the scattered parton. When $p_{\perp c}$ and s get large, however, both of these alternatives also give the result (1). The reason is that for $|p_{\perp}| > \mathcal{O}(\langle m_{\perp} \rangle)$, both alternative distributions become, when viewed in the center of mass of a and b , approximately straight cylinders pointing toward the origin, as in Fig. (6). Appreciable deviations from these asymptotes occur only when $|p_{\perp}| \lesssim \mathcal{O}(\langle m_{\perp} \rangle)$. But, this is the region where the parton cylinders begin to overlap the hadron cylinders lying along the p_{\parallel} axis. These corrections can only affect C_x or the finite pionization region near the origin, and therefore both these possibilities will result in asymptotic multiplicities given by Eq. (2.4). Notice that we do not mean to imply that these differences are moot or untestable; in fact, we believe they are quite important. We only mean that they all result in the same asymptotic expression for $\langle n \rangle_{\text{deep}}$.

We would now like to discuss some limitations and possible corrections to Eq. (2.4).¹⁴ First, our picture is not the correct one in the limit that the scattering angle of $c \rightarrow 0$, even though $p_{\perp c}$ gets large. In this limit, the central pionization region in Fig. (6) spreads out along the p_{\parallel} axis and forms an additional plateau which will significantly contribute to $\langle n \rangle$ of such events. As we shall see in Chapter III, the deep region may include values of p_{\perp} and s such that in the scattering angle of c goes to zero asymptotically, so this is an important qualification to bear in mind. Second, there may be corrections to our formula coming from events in which two partons scatter through a small angle in their center of mass. It is possible that such partons, if they communicate with the holes, will contribute $C_{e^+e^-} \ln P_{\perp p}$ to $\langle n \rangle$ rather than $C_{e^+e^-} \ln E_p$. If such a mechanism exists, it will alter our expression for $\langle n \rangle_{\text{deep}}$ in certain

kinematic regions. However, these corrections will become less important as the energy and scattering angle of the observed particle increase.

Another interesting experiment to consider is the semi-inclusive process $a + b \rightarrow c + d + X$ where both c and d come out with large $|p_{\perp}|$ in opposite hemispheres, each being produced by one of the isolated partons. From Fig. (6) we easily find that the multiplicity for this process is asymptotically given by

$$\begin{aligned} \langle n(s, E_c, E_d) \rangle_{\text{deep}} &= (C_{e^+e^-} + C_X) \ln E_c E_d + \theta(s - 16 E_c^2) C_h \ln \left(\frac{\sqrt{s}}{2 E_c} - 1 \right) \\ &+ \theta(s - 16 E_d^2) C_h \ln \left(\frac{\sqrt{s}}{2 E_d} - 1 \right) \end{aligned} \quad (2.5)$$

where, again, we have neglected the terms which remain finite as s, E_c and $E_d \rightarrow \infty$. Notice the similarity between this expression and expression (2.4) for the one particle inclusive case. However, in this experiment we can, on the average, deduce the energy of the partons which produce c and d if we know f_p (or, equivalently, $C_{e^+e^-}$). While this knowledge does not strongly affect the asymptotic relation (2.5), we can get a firmer handle on the possible corrections from small angle parton-parton scattering if we know E_p and $E_{p'}$. Furthermore, it is important to know the parton energies if we wish to derive non-asymptotic relationships between the multiplicities in deep hadron-hadron scattering and multiplicities in other high energy reactions. Let us turn now to a brief discussion of such relations.

We expect Eqs. (2.4) and (2.5) to be valid when clear hadronic and partonic plateaus in $\ln E$ have developed. In the absence of such plateaus, we cannot predict the s or p_{\perp} dependence of $\langle n \rangle$ since then the fragmentation region will play a major role, and their contributions to $\langle n \rangle$ depend in a more detailed way on

on specific (model-dependent) assumptions. However, we can try to relate $\langle n(s, E_c, E_d) \rangle$ to the multiplicities in other reactions. There are a number of detailed forms which such relations could take, but most simple options follow from one of four general arguments:

(1). In $e(\nu) - h$ scattering we remove a parton with energy E_p from the target hadron. We then have a hadron with a hole in it and a parton distant in momentum space. In whatever way the hole and liberated parton evolve in $l-h$ scattering, they do the same thing in deep $h-h$ scattering. If the results of Cahn, Cleymans and Colglazier⁸ are correct, this argument evaluated asymptotically predicts $C_x = C_{e^+e^-}$.

(2). The hole turns into hadrons just as the parton does. This also implies $C_x = C_{e^+e^-}$.

(3). The hole does not significantly affect the final hadron multiplicity so that the final hadron distribution along the p_{\parallel} axis looks as if no partons were removed. Then the p_{\parallel} distribution contributes to $\langle n \rangle_{\text{deep}}$ just the average multiplicity of an ordinary $h-h$ reaction. Asymptotically this gives $C_x = C_h$.

(4). The hole and parton dispose of themselves in similar ways, but these contributions to $\langle n \rangle_{\text{deep}}$ simply add to the contributions coming from the original hadrons sans holes.¹⁴ This argument predicts $C_x = C_h + C_{e^+e^-}$, asymptotically.

All of these arguments are plausible. While each is based on a seemingly different notion about the way parton distributions overlap and turn into hadrons, more than one may be correct. For instance, if $C_h = C_{e^+e^-}$, possibilities (1), (2) and (3) may all be true. On the other hand, it is possible that $C_h = C_{e^+e^-}$ with, say, only one of these arguments correct, nonasymptotically. It would indeed be very interesting to know which of the relations that follow from these

options are satisfied, and over what ranges of s and p_{\perp} . Tests of such expressions, as well as asymptotic determinations of C_x , C_h and $C_{e^+e^-}$ can yield much valuable information about the nature of partons and about the correct way to construct the amplitudes which describe the development of partons into final state hadrons.¹⁵

In this chapter we have presented a review of Feynman's version of the parton model and its application to the problem of average particle distributions and multiplicities in e^+e^- annihilation experiments, deep inelastic lepto-production, and ordinary hadron-hadron scattering. We have tried to extend these ideas to deep hadron-hadron scattering, and we have derived asymptotic formulae for the average multiplicities to be expected in such experiments. Although our arguments have been somewhat loose and heuristic, they have been based on notions which have been developed and applied to a number of different processes. As we have tried to show, the beauty and utility of this approach is its ability to correlate many a priori uncorrelated high energy processes by fairly simple, general arguments.

CHAPTER III

REGGE POLES IN DEEP HADRON-HADRON SCATTERING

A. Introduction

Recently, a number of theories have been proposed to explain the structure of inclusive and exclusive differential cross sections at large momentum transfers. The connection of at least some of these theories with the usual notions of Regge theory is rather obscure. For example, it is not obvious how to relate Regge theory to a theory in which partons play a role in the deep region, either by being scattered or being exchanged.

In this chapter, we will describe a general scheme which can connect theories of deep scattering with Regge theory for $2 \rightarrow 2$ amplitudes. Briefly, our approach consists of considering deep scattering amplitudes as Born terms and iterating them in the t-channel to build up moving Regge poles. We find that as $|t| \rightarrow 0$ graphs involving more and more Born terms in the t-channel become increasingly important, while as $|t| \rightarrow \infty$ the only graph which survives is the original deep-scattering amplitude. As we shall show, this approach unifies many of the intuitive features of a number of different theories: in particular, we see how the "hard" deep scattering interactions connect smoothly onto the "soft", coherent structures which dominate the Regge region. The existence of such a connection, furthermore, means that it is not necessary (indeed, it is not allowable) to introduce two different components, hard and soft, to describe hadron-hadron scattering. A field theory with hard interactions will automatically generate the coherent structure which is necessary to describe near forward scattering.

The chapter is organized as follows: in section B we derive and examine an integral equation (not unlike the Bethe-Salpeter equation) for the $2 \rightarrow 2$

amplitude which is obtained by summing graphs with various numbers of Born terms in the t-channel. Because section B is so long it is divided into five parts. In the first of these (subsection 1) we present a brief review of old-fashioned perturbation theory and the infinite momentum frame. In subsection 2, we give a covariant derivation of the integral equations and recursion relations on which we base the connection between the deep and Regge regions. Subsection 3 consists of a careful examination of these equations and what they imply for our Reggeization procedure. In subsection 4, we discuss some of the graphs which might be found in the Born term. This discussion illuminates the role played by various s and t-channel intermediate states in various kinematic regions. Section B concludes with subsection 5 in which we present an alternate derivation of our integral equation using old-fashioned perturbation theory rather than covariant perturbation theory (as used in subsection 2).

Turning to section C, we find a discussion of our Reggeization scheme for the case in which the scattering matrix has more than one (coupled) channel. Finally, in section D we show how to correctly incorporate signature into our problem. Furthermore, we apply our methods to the parton-interchange theory of deep scattering and end with some ideas about the relationship between parton-interchange diagrams and duality diagrams as well as some speculation about the dynamical origin of the Pomeron pole.

B. The Basic Integral Equation

1. Old Fashioned Perturbation Theory and the Infinite Momentum Frame.

In this section, we shall derive the integral equation which lies at the heart of our Reggeization procedure. Before beginning the actual derivation, however, it will be useful to review the simplest properties of the infinite

momentum frame (IMF) and its use in conjunction with old fashioned perturbation theory (OFPT).

As is well known, covariant perturbation theory is simply related to old fashioned perturbation theory. In OFPT, when working to some order in the couplings, one calculates a number of time ordered diagrams and adds them together to get the covariant scattering amplitude. In covariant perturbation theory, on the other hand, the use of Feynman propagators automatically ensures that all time orderings are included in the calculation of a single Feynman diagram. In a Feynman diagram with N vertices, there are in general $N!$ different time orderings for the N vertices, each one of which must be calculated separately in OFPT. Cast in these terms, the advantage of covariant perturbation theory in most calculations is evident.

There is a technique, however, which can restore the attractiveness of OFPT and give it a fighting chance for the affections of high energy theorists. This technique is the use of an infinite momentum frame. The usefulness of doing OFPT calculations in a special frame derives from the fact that the value of a given time ordered graph is not invariant. It is often possible to choose a frame in which only a few of the $N!$ graphs which contribute to some Feynman diagram are non-zero.

To illustrate the use of OFPT in the IMF, let us look at the crossed box diagram of Fig. (7). We wish to calculate this diagram in OFPT. In general we must consider the 24 different time orderings of the four vertices, and in an arbitrary frame all of them may contribute. Being clever physicists, however, we choose a frame in which all of the external particles are moving very fast to the right. Eventually, we shall let c approach very fast. We

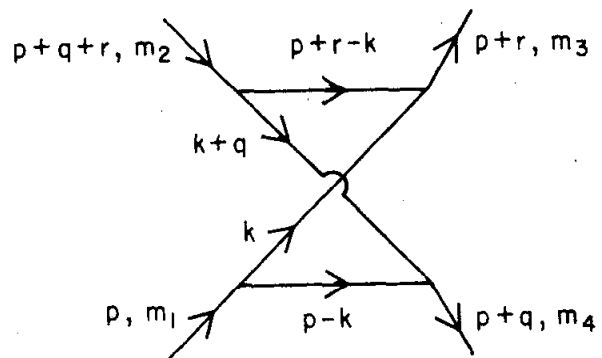


FIG. 7--Sample Feynman diagram for illustration of old-fashioned perturbation theory in the infinite momentum frame.

parameterize the momenta in our frame as follows:¹⁶

$$\begin{aligned}
 \mathbf{p} &= \left(\mathbf{P} + \frac{m_1^2}{2P}, 0, \mathbf{P} \right) \\
 \mathbf{q} &= \left(\frac{\mathbf{p} \cdot \mathbf{q}}{P}, \mathbf{q}_\perp, 0 \right) \\
 \mathbf{r} &= \left(\frac{\mathbf{p} \cdot \mathbf{r}}{P}, \mathbf{r}_\perp, 0 \right) \\
 \mathbf{k} &= \left(\mathbf{xP} + \frac{\mu^2 + k_\perp^2}{2xP}, \mathbf{k}_\perp, \mathbf{xP} \right)
 \end{aligned} \tag{3.1}$$

The mass of each internal line is μ . Since the energy of each internal particle is positive, we must have $0 < x < 1$ for sufficiently large P . The limit we are interested in is $P \rightarrow \infty$. Notice that in this limit $\mathbf{p}^2 = m_1^2$, as it should. When $P \rightarrow \infty$, the other external mass-shell conditions become:

$$\begin{aligned}
 (\mathbf{p} + \mathbf{r})^2 &= \left(\mathbf{P} + \frac{m_1^2 + 2\mathbf{p} \cdot \mathbf{r}}{2P}, \mathbf{r}_\perp, \mathbf{P} \right)^2 = m_1^2 + 2\mathbf{p} \cdot \mathbf{r} - \mathbf{r}_\perp^2 = m_3^2 \\
 (\mathbf{p} + \mathbf{q})^2 &= m_1^2 + 2\mathbf{p} \cdot \mathbf{q} - \mathbf{q}_\perp^2 = m_4^2 \\
 (\mathbf{p} + \mathbf{q} + \mathbf{r})^2 &= m_1^2 + 2\mathbf{p} \cdot \mathbf{q} + 2\mathbf{p} \cdot \mathbf{r} - (\mathbf{q}_\perp + \mathbf{r}_\perp)^2 = m_2^2
 \end{aligned} \tag{3.2}$$

Since $\mathbf{q}_\perp, \mathbf{r}_\perp$ do not depend on P , this shows explicitly that $\mathbf{p} \cdot \mathbf{r}$ does not depend on P , either. In this frame the Mandelstam variables become

$$\begin{aligned}
 t &= -\mathbf{q}_\perp^2 \\
 u &= -\mathbf{r}_\perp^2 \\
 s &= 2m_1^2 - 2m_2^2 + (\mathbf{q}_\perp + \mathbf{r}_\perp)^2
 \end{aligned} \tag{3.3}$$

where we have used the last equation in (3.2) in evaluating s . Adding together the three equations of (3.3) and using $s + t + u = \sum_i m_i^2$, we find the interesting relation

$$2q_{\perp} \cdot r_{\perp} = m_3^2 + m_4^2 - m_1^2 - m_2^2 \quad (3.4)$$

Let us now move on from kinematics, and evaluate diagram Fig. (7). In OFPT, one conserves three-momentum at each vertex and calculates time ordered diagrams according to the following rules (for spinless particles).¹⁷

(i) A factor $(E - E_j + i\epsilon)^{-1}$ for each intermediate state, j . E is the energy of the initial state, and E_j is the energy of the intermediate state.

(ii) An overall factor $-2\pi i \delta(E - E')$ where E' is the energy of the final state.

(iii) For each internal line an integration $\frac{1}{(2\pi)^3} \int \frac{d^3 p}{2p_0}$ where p_0 is the energy associated with the line.

(iv) For each vertex, a vertex function times $(2\pi)^3 \delta^3(p_{\text{out}} - p_{\text{in}})$. These rules give the s -matrix element $\langle f | S | i \rangle$ which is related to the invariant amplitude, \mathcal{M} , by $\langle f | S | i \rangle = (2\pi)^4 \delta^4(p_f - p_i) \mathcal{M}$ with the conventions Bjorken and Drell.

We may now proceed to calculate some of the time orderings of Fig. (7). Let us first look at the time ordering shown in Fig. (8). Calculating according to the rules above, we find

$$\mathcal{M} = \frac{g^4}{2(2\pi)^3} \int \frac{d^2 k_{\perp} dx}{x^2 (1-x)} \left[m_1^2 - \frac{\mu^2 + k_{\perp}^2}{x(1-x)} \right]^{-1} \left[m_1^2 - F - 4(1-x)P^2 \right]^{-1} \left[m_4^2 - \frac{\mu^2 + (k_{\perp} + (1-x)q_{\perp})^2}{x(1-x)} \right]^{-1} \quad (3.5)$$

where $F = m_1^2 - m_3^2 - r_\perp^2 - \frac{\mu^2 + k_\perp^2 + (r_\perp - k_\perp)^2}{1-x}$. The important thing to notice here is that there is a term $\propto P^{-2}$ coming from the middle energy denominator. Since the rest of the expression is independent of P (and finite), this time ordering will not contribute in the $P \rightarrow \infty$ limit. One can usually recognize such noncontributing graphs (at least in a spinless theory)¹⁸ by observing that they always have at least one line whose momentum is flowing the wrong way. In this case, it is the top horizontal line, as indicated by the arrow in Fig. (8).

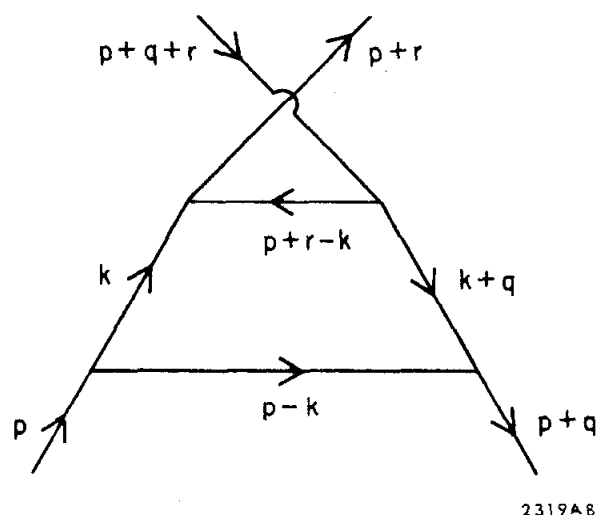
Continuing our analysis, we find that 20 of the 24 time orderings graciously vanish as $P \rightarrow \infty$ leaving the four time orderings shown in Fig. (9) with their energy denominators indicated by the dashed lines. To get the final covariant matrix element, we need only calculate these four time orderings and add them together. This is facilitated by the observation that the central energy denominator is the same in all four time orderings. The remaining pieces of each time ordering add together in a natural way, and the resultant expression for their sum is

$$\mathcal{M} = \frac{g^4}{2(2\pi)^3} \int \frac{d^2 k_\perp dx}{x^2 (1-x)^2} \Delta \left[m_1^2 - \tilde{S}(k_\perp, x) \right]^{-1} \left[m_2^2 - \tilde{S}(k_\perp + (1-x)q_\perp - xr_\perp, x) \right]^{-1} \left[m_3^2 - \tilde{S}(k_\perp - xr_\perp, x) \right]^{-1} \left[m_4^2 - \tilde{S}(k_\perp + (1-x)q_\perp, x) \right]^{-1} \quad (3.6)$$

where

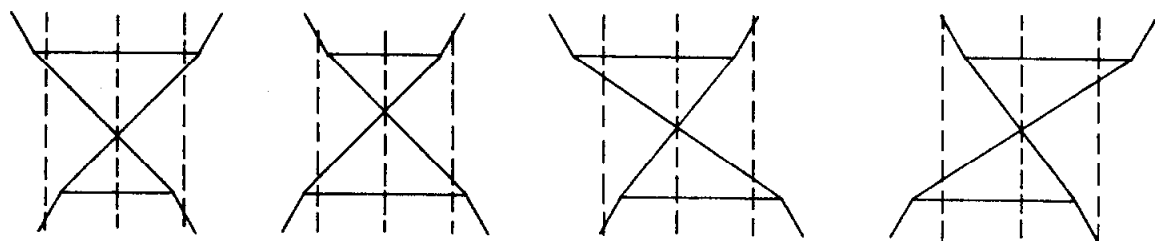
$$\tilde{S}(k_\perp, x) = \frac{k_\perp^2 + \mu^2}{x(1-x)}$$

and $\Delta \equiv m_1^2 + m_2^2 - \tilde{S}(k_\perp, x) - \tilde{S}(k_\perp + (1-x)q_\perp - xr_\perp, x)$



2319AB

FIG. 8--One of the 20 time orderings of Fig. 7 that vanish in the infinite momentum frame.



2319A9

FIG. 9--Time orderings of Fig. 7 that survive in the infinite momentum frame.

Δ is the central energy denominator which now appears in the numerator, and the four factors in the denominator are the energy differences across the four vertices. Notice that this expression for \mathcal{M} does not depend on P , and so survives the $P \rightarrow \infty$ limit.

The equivalence of this result with the evaluation of the corresponding Feynman diagram can be demonstrated in a straight-forward way using a procedure suggested by M. Schmidt.¹⁹ We shall only outline the method here since we shall discuss it in detail for a similar problem later in this section.

The technique consists of writing down the covariant Feynman expression and evaluating the dk^2 integral in the IMF. The Feynman amplitude for Fig. (7) is

$$\mathcal{M} = \int \frac{d^4 k}{i(2\pi)^4} \left[k^2 - \mu^2 + i\epsilon \right]^{-1} \left[(p-k)^2 - \mu^2 + i\epsilon \right]^{-1} \\ \left[(k+q)^2 - \mu^2 + i\epsilon \right]^{-1} \left[(p+r-k)^2 - \mu^2 + i\epsilon \right]^{-1} \quad (3.7)$$

With the parameterization of k in (3.1), we can make the transformation

$$\int d^4 k \rightarrow \int d^2 k_{\perp} \int_{-\infty}^{\infty} \frac{dx}{2|x|} \int_{-\infty}^{\infty} dk^2 \quad (3.8)$$

We now use (3.1) to write the propagators in (3.7) in terms of x , k_{\perp} and k^2 . The dk^2 integration can now be done using contour integrals. We find that all poles in the k^2 -plane are in the lower half plane unless $0 < x < 1$. Then, the integral for this range of x gives us back the expression (3.5).

2. Derivation of the Basic Equation

Having become facile in the use of OFPT in the IMF, let us turn to the problem of deriving the basic integral equation that Reggeizes large-angle

scattering. In what follows, we shall present two derivations of the equation. The one presented in this subsection will start from a Feynman diagram, and will use the trick outlined above. The second (subsection 5) will use OFPT from the outset. The first derivation is the more elegant, but the second can provide valuable insight into the Reggeization process within the context of parton models for large angle scattering.

To begin, we recall that our approach is to iterate two particle scattering amplitudes in the t-channel, and sum over the number of iterations in order to build up a moving Regge pole. The type of amplitude over which we shall sum is shown in Fig. (10). At the top of the ladder is a Born term, B , followed by j iterations of a $2 \rightarrow 2$ scattering amplitude, K . K and B may or may not be the same. This figure represents a term \mathcal{M}_j . The final Reggeized scattering amplitude is gotten by summing over j :

$$\mathcal{M} = \sum_{j=0}^{\infty} \mathcal{M}_j = B + \sum_{j=1}^{\infty} \mathcal{M}_j \quad (3.9)$$

It is convenient at this stage to derive a recursion relation between \mathcal{M}_{j+1} and \mathcal{M}_j . The equation we want is shown in Fig. (11). It can be written as

$$\begin{aligned} \mathcal{M}_{j+1}(u, t; \nu^2, \nu'^2; r^2, (q+r)^2) &= \int \frac{d^4 \ell}{i(2\pi)^4} \left[\ell^2 - M^2 + i\epsilon \right]^{-1} \left[(\ell+q)^2 - M^2 + i\epsilon \right]^{-1} \\ &\times K(u', t; \nu^2, \nu'^2; \ell^2, (\ell+q)^2) \mathcal{M}_j(\bar{u}, t; \ell^2, (\ell+q)^2; r^2, (q+r)^2) \quad (3.10) \end{aligned}$$

where $\nu^2 = p^2$, $\nu'^2 = (p+q)^2$, $u = (p-r)^2$, $t = q^2$, $\bar{u} = (\ell-r)^2$ and $u' = (p-\ell)^2$.

Notice that we have changed the labellings of the momenta from our previous example.

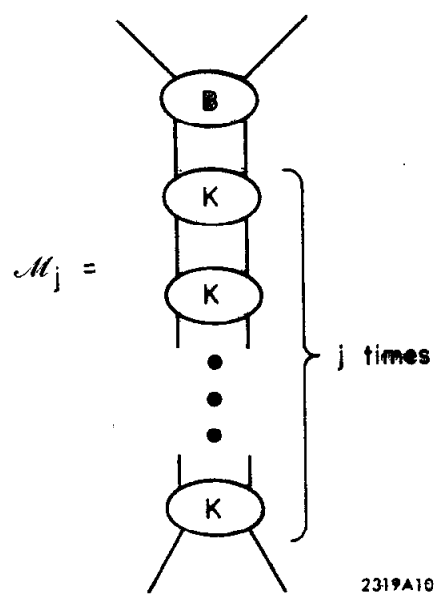
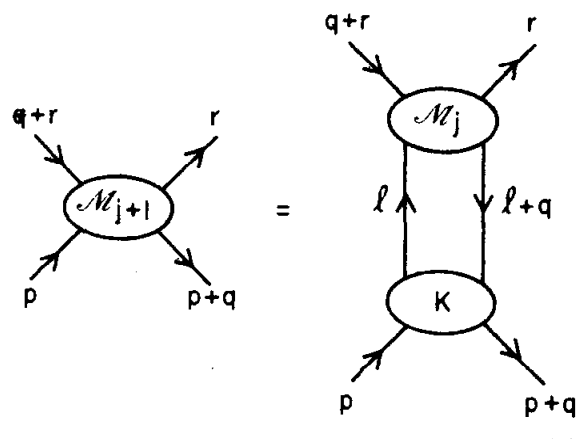


FIG. 10 - Graphical illustration of amplitude, \mathcal{M}_j .



2319A11

FIG. 11--The recursion relation connecting
 \mathcal{M}_{j+1} with \mathcal{M}_j .

At this point, we wish to introduce a dispersion relation for K in the variable u' . We can write

$$K(u', t', N^2, \Lambda^2) = \int d\sigma^2 \frac{W(\sigma^2, t, N^2, \Lambda^2)}{u' - \sigma^2 + i\epsilon} \quad (3.11)$$

where we have set $\lambda^2 = \ell^2$ and $\lambda'^2 = (\ell+q)^2$. Also, the capital N^2 and Λ^2 in the arguments of K and W indicate dependence on both ν^2 and ν'^2 , and λ^2 and λ'^2 respectively. We shall use this convention from now on. The reason for choosing such a representation for K will become clearer as we go along. For the time being, we only want to make three remarks. First, one must keep an open mind about how the $d\sigma^2$ contour is supposed to be performed in σ^2 -plane. Naively, one expects that the discontinuities of the integral in (3.11) are given by the denominator, and so the $d\sigma^2$ integral is performed by integrating along a line near the real σ^2 -axis. However, because of the dependence of W on the off-shell variables λ^2 and λ'^2 , it may be necessary to deform the $d\sigma^2$ contour away from the real axis and pick up contributions from complex singularities.²⁰ This is a way of incorporating possible diagrams in which the mass λ^2 or λ'^2 can become sufficiently time-like and is allowed to freely decay to internal lines. We shall have more to say about this situation as we proceed.

Second, in order to give the reader some idea of the forms one may expect W to take, we remark that for large $|u'|$ and $|t|$, a (tu) graph in the parton interchange theory of Gunion, Brodsky and Blankenbecler²¹ gives an expression for K like

$$K \sim f(t) (m^2 - u')^{-n}$$

if all external particles are on the mass shell. m is some finite mass

parameter. The W that reproduces such a K has the form

$$W \sim f(t) \frac{\delta^{[n-1]} (m^2 - \sigma^2)}{(n-1)!} \quad (3.12)$$

Of course, K does in general depend on the off-shell variables, Λ^2 , but bearing in mind the possibility of complex singularities, this functional form for W is probably not a bad ansatz as we shall see later.

The final comment we wish to make here is that in this and the next sections we shall, for simplicity, assume that there are singularities of K in u' only for positive u' when the external masses are on-shell. (Actually, when we use our ansatz to explicitly calculate the trajectories, we shall implicitly assume that this is also true when Λ^2 goes off-shell. That this latter is a reasonable assumption for K will become clear when we examine some simple kernels in subsection 4.) This will have the consequence that all the amplitudes we shall deal with will be purely real. Furthermore, such a singularity structure for K will generate a singularity in \mathcal{M}_j at positive u (or \bar{u} if \mathcal{M}_j appears under an integral). In Regge language, the means that the trajectories we generate will not have a rotating phase part in their signature factors. That is, each trajectory will really represent a pair of strongly exchange degenerate trajectories. In section D, we will extend the discussion to kernels involving other singularities, when we examine the relation of our work to duality diagrams.

With these remarks in mind, let us continue with the derivation of our recursion relation. Inserting (3.11) into (3.10), we have

$$\begin{aligned} \mathcal{M}_{j+1}(u, t; N^2, R^2) &= \int \frac{d^4 \ell}{i(2\pi)^4} d\sigma^2 \left[\ell^2 - M^2 + i\epsilon \right]^{-1} \left[(\ell+q)^2 - M^2 + i\epsilon \right]^{-1} \left[(P-\ell)^2 - \sigma^2 + i\epsilon \right]^{-1} \\ W(\sigma^2, t; N^2, \Lambda^2) \mathcal{M}_j(\bar{u}, t; \Lambda^2, R^2) \end{aligned} \quad (3.13)$$

Where R^2 stands for the variables r^2 and $(q+r)^2$.

We evaluate (3.13) by the trick outlined above. We choose an infinite momentum frame and parameterize the momenta as follows:

$$\begin{aligned}
 p &= \left(P + \frac{\nu^2}{2P}, 0, P \right) \\
 q &= \left(\frac{q \cdot p}{P}, q_\perp, 0 \right) \\
 r &= \left(\frac{r \cdot p}{P}, r_\perp, 0 \right) \\
 \ell &= \left(yP + \frac{\ell^2 + \ell_\perp^2}{2yP}, \ell_\perp, yP \right)
 \end{aligned} \tag{3.14}$$

Again we have in mind the limit $P \rightarrow \infty$. With this notation,

$$u = (p-r)^2 = \nu^2 + r^2 - 2p \cdot r, \quad t = q^2 \text{ and } s = (p+q+r)^2 = \nu^2 + (q+r)^2 + 2p \cdot q + 2p \cdot r.$$

Since these are invariants they cannot depend on P . This shows explicitly that $p \cdot r$ and $p \cdot q$ are independent of P . The observant reader will immediately notice that this means that the two external masses r^2 and $(q+r)^2$ are space-like. This is a convenient choice for our problem, and will cause no difficulty since the final matrix element will be analytic in the external masses, and we will be able to continue q^2 and $(q+r)^2$ to stable physical masses.

The next step is to transform the $d^4\ell$ integral in (3.13) and pick out the singularities in ℓ^2 . Using (3.14), we now introduce a dispersion relation for \mathcal{M}_j similar to (3.11) which is for K . We write

$$\mathcal{M}_j(\bar{u}, t; \Lambda^2, R^2) = \int d\rho^2 \frac{W_j(\rho^2, t; \Lambda^2, R^2)}{\bar{u} - \rho^2 + i\epsilon} \tag{3.15}$$

The remarks made below (3.11) apply here also — we must keep an open mind about the location of the path of integration in the ρ^2 -plane.

Now we wish to insert (3.15) into (3.13) and perform part of the $d^4\ell$ integration. Using (3.14), we easily carry out the transformation

$$\int d^4\ell = \int_{-\infty}^{\infty} \frac{dy}{2|y|} \int d^2\ell_{\perp} \int_{-\infty}^{\infty} d\ell^2$$

We can expand the four propagators which now appear in (3.13) (because we have used (3.15)) and perform the $d\ell^2$ integral by locating their poles in ℓ^2 .

Using (3.14), we easily verify that the pole from the propagator in (3.15) is always in the lower half ℓ^2 -plane. As for the other three propagators, we have

$$\begin{aligned} [\ell^2 - M^2 + i\epsilon] &= [\ell^2 - M^2 + i\epsilon] \\ [(\ell + q)^2 - M^2 + i\epsilon] &= [\ell^2 + 2yP \cdot q - 2q_{\perp} \cdot \ell_{\perp} + q^2 - M^2 + i\epsilon] \\ [(P - \ell)^2 - \sigma^2 + i\epsilon] &= \left[(1 - \frac{1}{y}) \ell^2 + (1-y) \nu^2 - \frac{\ell_{\perp}^2}{y} - \sigma^2 + i\epsilon \right] \end{aligned}$$

If $(1 - \frac{1}{y}) > 0$ all the poles from these factors also lie in the lower-half ℓ^2 -plane. Closing the contour in the upper half plane, we get zero. If $(1 - \frac{1}{y}) < 0$ ($\rightarrow 0 < y < 1$), the propagator from the dispersion representation of K is in the upper half plane, and so we pick up a non-zero contribution for this range of y . Carrying out the $d\ell^2$ integration therefore gives

$$\begin{aligned} \mathcal{M}_{j+1}(u, t; N^2, R^2) &= \frac{1}{2(2\pi)^3} \int d\sigma^2 d\rho^2 \int_0^1 \frac{dy d^2\ell_{\perp}}{(1-y)} \left[\lambda^2 - M^2 + i\epsilon \right]^{-1} \\ &\quad \left[\lambda'^2 - M^2 + i\epsilon \right]^{-1} \left[\bar{u} - \rho^2 + i\epsilon \right]^{-1} W(\sigma^2, t; N^2, \Lambda^2) W_j(\rho^2, t; \Lambda^2, R^2) \end{aligned} \quad (3.16)$$

where now

$$\begin{aligned}\bar{u}^2 - M^2 &= y \left[u - S(\ell_{\perp} - (1-y) r_{\perp}, y) \right] \\ \lambda^2 - M^2 &= y \left[\nu^2 - S(\ell_{\perp}, y) \right] \quad (3.17)\end{aligned}$$

and

$$\lambda'^2 - M^2 = y \left[\nu'^2 - S(\ell_{\perp} + (1-y) q_{\perp}, y) \right],$$

with $S(\ell_{\perp}, y) \equiv \frac{1}{y(1-y)} \left[\ell_{\perp}^2 + (1-y) M^2 + y \sigma^2 \right].$

S as defined here is similar to \tilde{S} as defined in (3.6), the difference being the appearance of the off-shell mass, σ^2 , in the present case.

It is instructive to rewrite (3.16) in a way that makes its connection with OFPT calculations more apparent. Using (3.17), we can write (3.16) as

$$\begin{aligned}\mathcal{M}_{j+1}(u, t; N^2, R^2) &= \frac{1}{2(2\pi)^3} \int d\sigma^2 d\rho^2 \int_0^1 \frac{dy d^2 \ell_{\perp}}{y^3 (1-y)} \left[\nu^2 - S(\ell_{\perp}, y) \right]^{-1} \\ &\left[\nu'^2 - S(\ell_{\perp} + (1-y) q_{\perp}, y) \right]^{-1} \left[u - S'(\ell_{\perp} - (1-y) r_{\perp}, y) \right]^{-1} W(\sigma^2, t; N^2, \Lambda^2) \\ &W_j(\rho^2, t; \Lambda^2, R^2). \quad (3.18)\end{aligned}$$

where

$$S'(\ell_{\perp}, y) \equiv \frac{1}{y(1-y)} \left[\ell_{\perp}^2 + (1-y) \rho^2 + y \sigma^2 \right].$$

To interpret this form we refer the reader to Fig. (12). If we set both W 's equal to δ -function in (3.18), i.e.,

$$W(\sigma^2) W_j(\rho^2) \rightarrow \delta(\mu^2 - \sigma^2) \delta(\mu^2 - \rho^2)$$

The right-hand side would be exactly the OFPT expression for the crossed box diagram evaluated in our IMF. Notice that because of the judicious choice of space-like values for r^2 and $(q+r)^2$ only one time-ordering survives. The three factors in square brackets are just the three energy denominators which appear in this remaining diagram. Therefore, the right-hand side of (3.18) is the crossed box diagram evaluated in the IMF and convoluted with weight functions that measure the spectrum of the horizontal lines, as shown in Fig. (12).

A few remarks are in order about equations (3.16) and (3.18). First, the reader will surely have noticed that we never considered possible singularities in the ℓ^2 -plane from the dependence of the weight functions, W and W_j , on the off-shell masses λ^2 and λ'^2 . The reason is that while there are such singularities in the off-shell amplitudes, K and M_j , they do not appear in the imaginary parts, W and W_j . This was realized in another context by a number of smart men at Princeton when I was 13 years old.²⁰ If one continues the external masses Λ^2 to large time-like values, one is in general required to deform the path of integration in the σ^2 (or ρ^2) plane to avoid complex singularities in σ^2 (ρ^2) which appear in W (W_j). However, this does not introduce extra singularities in the ℓ^2 -plane until after we perform the $d\sigma^2(d\rho^2)$ integral. Then, of course, the singularities are in $K(M_j)$, and not their imaginary parts. In subsection 4, we will present an example of a kernel for which this sort of thing occurs, and we shall then present a graphical explanation of these statements.

The equations (3.16) and (3.18) are exact recursion relations for the scattering amplitudes which contain j t-channel iterations of an irreducible kernel. Now, there is evidently nothing stopping us from formally redoing the $d\rho^2$ integral (with the proper choice of the path of integration). Doing this in (3.16), and

$$\begin{array}{c}
 \text{Diagram of } M_{j+1}: \text{An oval with } M_{j+1} \text{ inside, connected to three lines.} \\
 = \int d\sigma^2 d\rho^2 W(\sigma^2) W_j(\rho^2) \times \\
 \text{Diagram of spectral function: A triangle with } \rho^2 \text{ on the top edge and } \sigma^2 \text{ on the bottom edge.}
 \end{array}$$

2319A12

FIG. 12--The recursion relation in terms of integrals over the spectral functions of the subamplitudes.

using (3.15), we have

$$\mathcal{M}_{j+1}(u, t; N^2, R^2) = \frac{1}{2(2\pi)^3} \int_0^1 dy \frac{dy d^2 \ell_\perp d\sigma^2}{y^2(1-y)} \left[\lambda^2 - M^2 + i\epsilon \right]^{-1} \left[\lambda'^2 - M^2 + i\epsilon \right]^{-1} W(\sigma^2, t; N^2, \Lambda^2) \mathcal{M}_j(\bar{u}, t; \Lambda^2, R^2) \quad (3.19a)$$

which is also an exact recursion relation. Using (3.18), we can also write this as

$$\mathcal{M}_{j+1}(u, t; N^2, R^2) = \frac{1}{2(2\pi)^3} \int_0^1 \frac{dy d^2 \ell_\perp d\sigma^2}{y^2(1-y)} \left[\nu^2 - S(\ell_\perp, y) \right]^{-1} \left[\nu'^2 - S(\ell_\perp + (1-y)q_\perp, y) \right]^{-1} W(\sigma^2, t; N^2, \Lambda^2) \mathcal{M}_j(\bar{u}, t; \Lambda^2, R^2) \quad (3.19b)$$

To perform the final (trivial) step in the derivation of our integral equation, we sum both sides of (3.19a) over j from zero to infinity. Doing this, we have

$$\mathcal{M}(u, t; N^2, R^2) = B(u, t; N^2, R^2) + \frac{1}{2(2\pi)^3} \int_0^1 \frac{dy d^2 \ell_\perp d\sigma^2}{1-y} \left[\lambda^2 - M^2 + i\epsilon \right]^{-1} \left[\lambda'^2 - M^2 + i\epsilon \right]^{-1} W(\sigma^2, t; N^2, \Lambda^2) \mathcal{M}(\bar{u}, t; \Lambda^2, R^2) \quad (3.20)$$

with \mathcal{M} defined as in (3.9). This equation is depicted in Fig. (13).

Because it is so useful, we wish to display this equation another way. Using (3.19b), we easily find

$$\mathcal{M}(u, t; N^2, R^2) = B(u, t; N^2, R^2) + \frac{1}{2(2\pi)^3} \int_0^1 \frac{dy d^2 \ell_\perp d\sigma^2}{y^2(1-y)} \left[\nu^2 - S(\ell_\perp, y) \right]^{-1} \left[\nu'^2 - S(\ell_\perp + (1-y)q_\perp, y) \right]^{-1} W(\sigma^2, t; N^2, \Lambda^2) \mathcal{M}(\bar{u}, t; \Lambda^2, R^2) \quad (3.21)$$

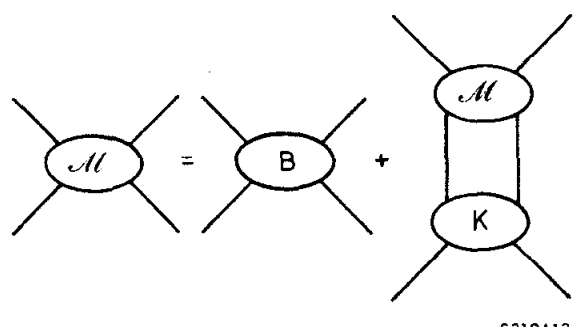


FIG. 13--The full integral equation.

3. The Reggeization Procedure

These are the equations that lie at the heart of our Reggeization procedure. We would now like to analyze the behavior of the solutions given the Born term, B , and the kernel, K . Notice that both sides of equation (3.21) are evaluated at a fixed value of t . In principle, therefore, we need to know B and K at all values of t in order to determine $M(t)$.²² However, since our approach is to Reggeize the deep scattering region, it is natural to begin by examining (3.21) for large $|t|$.

Measurements of differential cross sections at large angles²³ indicate a power law behavior both in s and t . Matrix elements which describe large angle scattering must therefore reflect this behavior, and a number of theories of deep scattering²⁴ have been proposed to describe these gross properties. A simple expression which may be taken as an approximation to the results of some of these models is a form alluded to earlier:

$$B = f(t) (\mu^2 - u)^{-n} \quad (3.22)$$

As our notation indicates, we wish to regard such a function as a Born term. In fact, we will also use it for the function K . At this point, such a form may be regarded as a general and reasonably accurate ansatz based partly on phenomenology and partly on features which are common to a number of models. Later, however, especially in Section D, we will call upon the parton-interchange model²¹ for a more specific interpretation of the Born term.

In the present calculation, the expression (3.22) is intended to be purely real. Actually, we could have chosen any number of similar forms for B , some of which would have imaginary parts, and in certain $2 \rightarrow 2$ amplitudes other forms for B may be more appropriate. But, as we have stated before, we wish to

confine ourselves in this and the next sections to the simplest possible cases. Furthermore, (3.22) is physically relevant since it is the Born term expected from the parton interchange theory for exotic reactions such as p-p elastic scattering where only a (tu) quark interchange graph is allowed.

To begin Reggeizing the Born Term, (3.22), let us examine first the amplitude \mathcal{M}_1 in the series which sums to \mathcal{M} . Using (3.19b), we have

$$\mathcal{M}_1(u, t, N^2, R^2) = \frac{f^2(t)}{2(2\pi)^3(n-1)!} \int_0^1 \frac{dy d^2\ell_\perp d\sigma^2}{y^2(1-y)} \left[\nu^2 - S(\ell_\perp, y) \right]^{-1} \left[\nu'^2 - S(\ell_\perp + (1-y)q_\perp, y) \right]^{-1} \delta^{[n-1]}(\mu^2 - \sigma^2)(\mu^2 - u)^{-n} \quad (3.23)$$

where we have used the fact that

$$\begin{aligned} K(u', t; N^2, \Lambda^2) &= f(t)(\mu^2 - u')^{-n} = \int \frac{d\sigma^2 W(\sigma^2, t; N^2, \Lambda^2)}{u' - \sigma^2 + i\epsilon} \\ &= \frac{1}{(n-1)!} \int \frac{d\sigma^2 f(t) \delta^{[n-1]}(\mu^2 - \sigma^2)}{u' - \sigma^2 + i\epsilon} \end{aligned}$$

and so

$$W(\sigma^2, t; N^2, \Lambda^2) = \frac{f(t)}{(n-1)!} \delta^{[n-1]}(\mu^2 - \sigma^2). \quad (3.24)$$

The superscript on the δ -function refers to the number of derivatives of the δ -function. For simplicity, we have assumed that n is an integer. (This result was mentioned earlier in (3.12). We wish to examine (3.23) in the large $|u|$ limit. To do this it is first convenient to Feynman parameterize the denominators. Using the well-known Feynman integral, we easily derive

the identity

$$\left[D_1 D_2 D_3^n \right]^{-1} = n(n+1) \int_0^\infty d\alpha_1 d\alpha_2 d\alpha_3 \delta(1-\alpha_1-\alpha_2-\alpha_3) \alpha_3^{n-1} \\ \left[\alpha_1^{D_1} + \alpha_2^{D_2} + \alpha_3^{D_3} \right]^{-(n+2)}$$

by differentiation with respect to D_3 . Using this in (3.23), we find after some simplification,

$$\mathcal{M}_1(u, t) = \frac{n(n+1)f^2(t)}{2(2\pi)^3(n-1)!} \int dy (1-y)^{n+1} d^2 \ell_\perp d\sigma^2 \delta^{[n-1]}(\mu^2 - \sigma^2) \\ d\alpha_1 d\alpha_2 d\alpha_3 \delta(1-\alpha_1-\alpha_2-\alpha_3) \alpha_3^{n-1} \left[\rho'^2 + \ell_\perp^2 + (1-y)^2 \alpha_1 \alpha_2 q_\perp^2 - y(1-y) \alpha_3 u + y \sigma^2 \right]^{-(n+2)} \quad (3.25)$$

with

$$\rho'^2 = (1-y) \left[(\alpha_1 + \alpha_2) M^2 + \alpha_3 \mu^2 \right] - y(1-y) \left[\alpha_1 \nu^2 + \alpha_2 \nu'^2 \right] + (1-y)^2 \alpha_3 \left[\alpha_1 r_\perp^2 + \alpha_2 (q_\perp + r_\perp)^2 \right]$$

ρ'^2 is a mass parameter, which is independent of $t = -q_\perp^2$ and u . Incidentally, this form clearly demonstrates the analytic dependence of \mathcal{M}_1 on the external masses, in particular $-r_\perp^2$ and $-(q_\perp + r_\perp)^2$. Also, it is interesting to notice the expected symmetry under the interchange $r_\perp^2 \leftrightarrow (q_\perp + r_\perp)^2$ and $\nu^2 \leftrightarrow \nu'^2$.

The next step is to perform the $d^2 \ell_\perp$ and $d\sigma^2$ integrals. The $d^2 \ell_\perp$ integration is easily carried out. The $d\sigma^2$ integration is done by integrating by parts $(n-1)$ times. The result of these two operations is

$$\mathcal{M}_1(u, t) = \frac{\pi(-1)^n \Gamma(2n)}{\Gamma^2(n) 2(2\pi)^3} f^2(t) I(u, t) \quad (3.26)$$

where

$$I(u, t) = \int_0^\infty dx dy d\alpha d\beta \delta(1-x-y-\alpha-\beta) (xy)^{n-1} \left[\rho^2 - \alpha\beta t - xyu \right]^{-2n}$$

and

$$\rho^2 = \rho'^2 + y\mu^2$$

We have defined $x = (1-y)\alpha_3$, $\alpha = (1-y)\alpha_1$, and $\beta = (1-y)\alpha_2$. The y -integral may be extended to ∞ , since as long as α , β , and x are positive, the region $y > 1$ cannot contribute because of the δ -function.

To examine the leading behavior of \mathcal{M}_1 for large $|u|$, we can use a Mellin transform technique. Actually, there are two problems to which we must address ourselves. We need to consider both the limits $|u| \rightarrow \infty$ with $t/u \rightarrow 0$, and $|u| \rightarrow \infty$ with t/u fixed. The latter is the asymptotic fixed angle region. While we expect that the leading behavior in these limits will be simply related, it is not a priori obvious what that relation is.

Let us proceed, then, by writing the integral in (3.26) in terms of its double Mellin transform in the variables $-u$ and $-t$.

$$I(u, t) = \left(\frac{1}{2\pi i} \right)^2 \int_{a-i\infty}^{a+i\infty} ds |u|^{-s} \int_{b-i\infty}^{b+i\infty} dr |t|^{-r} G(s, r) \quad (3.27)$$

a (b) must be chosen so that the contour in the s (r) plane does not pass over any singularities of G . It is easy to see that $I(u, t)$ is finite if $|u|$ and/or $|t| \rightarrow 0$, and $I \rightarrow 0$ if $|u|$ and/or $|t| \rightarrow \infty$, so we may choose both a and b just to the right of zero in their respective complex planes. Equation (3.27) can be inverted to obtain an expression for $G(s, r)$ according to the formula

$$G(s, r) = \int_0^\infty d|u| |u|^{s-1} \int_0^\infty d|t| |t|^{r-1} I(u, t) \quad (3.28)$$

Because of the simple form of the integral in (3.26), the $|u|$ and $|t|$ integrations can be readily carried out, and we find

$$G(s, r) = \frac{\Gamma(s) \Gamma(r) \Gamma(2n-s-r)}{\Gamma(2n)} \int_0^\infty dx dy d\alpha d\beta (xy)^{n-s-1} (\alpha\beta)^{-r} \times \delta(1-x-y-\alpha-\beta) (\rho^2)^{s+r-2n} \quad (3.29)$$

To get this form, it is necessary that (3.28) exist. This translates into the conditions $s < n$ and $r < 1$, which is consistent with $\text{Re } s$ and $\text{Re } r$ being to the right of zero, as we needed above, since $n \geq 1$.

To pick out the leading behavior of \mathcal{M}_1 , we need to find the singularities of G in s and r . For simplicity, we shall set all the external masses equal to zero, and let $\mu^2 = M^2$. Then $\rho^2 = \mu^2$, and it will be easy to examine the singularities of G . If we generalize to arbitrary, stable external masses and unequal internal masses, it becomes somewhat more complicated to analyze (3.28), but the singularity structure will not change since ρ^2 is always finite and non-zero.

If we introduce the representation for the δ -function

$$\delta(x) = \frac{1}{2\pi} \int_{-\infty}^{\infty} d\omega e^{i\omega x}$$

into (3.28), we can carry out the integrals over x , y , α and β . To do this, we give ω a small negative imaginary part, which will go to zero at the end of the calculation. Using

$$\int_0^\infty dx x^{A-1} e^{-i(\omega-i\epsilon)x} = (\epsilon + i\omega)^{-A} \Gamma(A)$$

we have

$$G(s, r) = \frac{(\mu^2)^{s+r-2n} \Gamma(s) \Gamma(r) \Gamma(2n-s-r)}{\Gamma(2n)} \Gamma^2(n-s) \Gamma^2(1-r) \\ \times \int_{-\infty}^{\infty} d\omega (\epsilon + i\omega)^{-2[(n-s)+(1-r)]} e^{i\omega}$$

The last integral is easily done,²⁵ and the limit $\epsilon \rightarrow 0$ presents no difficulty. We finally have

$$G(s, r) = 2\pi(\mu^2)^{s+r-2n} \frac{\Gamma^2(n-s) \Gamma^2(1-r) \Gamma(s) \Gamma(r) \Gamma(2n-s-r)}{\Gamma(2n) \Gamma[2(n-s+1-r)]} \quad (3.30)$$

Now we would like to discuss the singularities of G in s for fixed r . The singularities at the smallest value of s will give the leading contribution to M , at large $|u|$. We start off, therefore, with r near zero, and increase s along the positive s -axis. Since $n \geq 1$, the first singularity we hit is evidently a pole at $n = s$ coming from $\Gamma^2(n-s)$. Let us expand G in s about $s = n$. Using the expansion,

$$\Gamma(z + \epsilon) = \Gamma(z) [1 + \epsilon \psi(z)] + \mathcal{O}(\epsilon^2); \quad z \neq 0, -1, -2, \dots$$

we find for s near n ,

$$G(s, r) \approx 2\pi(\mu^2)^{r-n} \frac{\Gamma^2(1-r) \Gamma(r) \Gamma(n) \Gamma(n-r)}{\Gamma(2n) \Gamma(2-2r)} \\ \times \left\{ (n-s)^{-2} + (n-s)^{-1} \left[2\psi(1) + \psi(n) + \psi(n-r) - 2\psi(2-2n) - \ln\mu^2 \right] \right\} \quad (3.31)$$

There is therefore both a double pole and a single pole at $s = n$. To see what this formula implies for the asymptotic behavior of I in $|u|$, we need only use (3.27) and perform the inverse Mellin transform in s .

Now, for large $|u|$, the s contour integral in (3.27) should be closed in the right-half plane so that $|u|^{-s} = e^{-s \ln|u|}$ will provide convergence to the integral. We can then let a go from zero to $n + \epsilon$, and we will explicitly pick up the poles at $s = n$ which are the left-most singularities for $s > 0$. Now, it is easy to show using the Cauchy formula that

$$\frac{1}{2\pi i} \oint ds |u|^{-s} (n-s)^{-(m+1)} = \frac{(-1)^{m+1}}{m!} |u|^{-n} \ln^m |u| \quad (3.32)$$

It is clear then that the leading behavior for $|u| \rightarrow \infty$ comes from these left-most singularities. The behavior of $I(u, t)$ for large $|u|$ may thus be written as

$$I(u, t) = \tilde{R}_1(t) |u|^{-n} \ln|u| + \tilde{R}_0(t) |u|^{-n}; \quad |u| \rightarrow \infty$$

where the \tilde{R} 's are obtained by performing the r -integral of (3.27). The leading behavior of \mathcal{M}_1 then follows from (3.26) and can be written as

$$\mathcal{M}_1(u, t) = f(t) R_1(t) (-u)^{-n} \ln(-u) + f(t) R_0(t) (-u)^{-n} \quad (3.33)$$

The appearance of a term $\propto \ln|u|$ is the major feature of interest here. This term begins a sum of ever increasing powers of $\ln|u|$ which Reggeizes the large-angle Born term and turns the fixed pole in u into a moving pole that depends on t . But more about that later. For the moment we return to the expression (3.33) and note that, strictly speaking, we have only shown that this is the correct asymptotic behavior of \mathcal{M}_1 when $|u|$ is the only parameter which goes to infinity; that is, when $|t|$ is fixed (but not necessarily small). We would now like to examine the behavior of \mathcal{M}_1 when $|t|$ is allowed to grow, also. To do this we must go back to the exact expression for G (3.30) and examining the singularities of G in r as well as s . If we try to use (3.33) and examine the singularities

of the integrals which give the factors $R(t)$ we will get the wrong numerical factors, since the expansion above (3.31) is not valid at the poles of $\Gamma(z)$.

Examining (3.30), it is easy to see that the first singularities of G for positive r are poles at $r = 1$. We can expand this expression simultaneously about $r = 1$ and $s = n$. When we do this, we need to consider separately the two cases $n = 1$ and $n > 1$. It is straightforward to calculate the terms of interest exactly, but for our purposes it is sufficient to notice what the form of the leading singularities is. Remembering that $\Gamma(x) \sim x^{-1}$ for small x , we can simply count the order of the leading poles at $r = 1$ and $s = n$ in the expression (3.30) for G . Using (3.26), (3.27) and (3.32), we can then translate this singularity structure into the asymptotic behavior of \mathcal{M}_1 . Doing this, we easily find that for large $|u|$ and $|t|$,

$$\begin{aligned} \mathcal{M}_1(u, t) &= \frac{f^2(t)}{(-u)(-t)} \left[A_1 \ln(-u) \ln(-t) + A_2 [\ln(-u) + \ln(-t)] + A_3 \right] ; \quad n = 1 \\ &= \frac{f^2(t)}{(-u)^n(-t)} \left[B_1 [\ln(-u) + \ln(-t)] + B_2 \right] ; \quad n > 1 \end{aligned} \quad (3.34)$$

where the A_i and B_i are independent of u and t . The fact that the expression in large square brackets for the case $n=1$ is symmetric in u and t follows from the symmetry of $I(u, t)$ for $n=1$, and has been personally verified by explicit calculation. Notice also that for $n > 1$ the coefficients of $\ln(-u)$ and $\ln(-t)$ are equal. These expressions are valid asymptotic formulae when $|u|$ and $|t|$ are both large. In particular, when $|u| \rightarrow \infty$, (3.34) is valid for large $|t|$ whether $t/u \rightarrow 0$ or not. We would also like to point out that unlike the large $|u|$ behavior (3.33), the large $|t|$, large $|u|$ behavior (3.34) of \mathcal{M}_1 is not easily obtained by direct inspection of (3.26), thus underlining the utility of the Mellin transform technique.

Now, $f^2(t)$ is generally expected to fall for large $|t|$ — at the worst, $f(t) = \text{constant}$ for a simple ladder graph with point couplings. Comparing the term \mathcal{M}_1 with the Born term (3.22), we see that as $|t|$ gets large, \mathcal{M}_1 falls with respect to \mathcal{M}_0 by at least one power of $|t|$ (mod logs). This is fortunate, since the spirit of our approach is to assume that the Born term adequately describes the deep scattering region, and so the other graphs in the theory should become negligible in this region. We shall return to (3.34) below when we discuss the definition of the deep region, and the asymptotic behavior of the trajectory function $\alpha(t)$, but for now let us continue building and summing ladder-like graphs.

To convincingly establish that our sum will Reggeize, we must examine the leading behavior of \mathcal{M}_2 for $|u| \rightarrow \infty$. Using (3.19b), (3.33) and the expression for our kernel, we can obtain an expression for \mathcal{M}_2 . In using (3.33) for \mathcal{M}_1 , we are of course assuming that the important region of integration in (3.19b) is such that \bar{u} is large so that the asymptotic formula for \mathcal{M}_1 is applicable. In fact, it is also necessary that this condition be satisfied in generating \mathcal{M}_1 from the two iterated Born terms, since the Born terms are intended to describe high energy (deep) scattering. We shall show below that this condition is fulfilled, but for the time being let us assume that no swindle is being perpetrated, and proceed.

Since we expect to need $\mathcal{M}_1(\bar{u})$ for large \bar{u} , it will be convenient to examine only the leading term $\sim |\bar{u}|^{-n} \ln |\bar{u}|$. (The reader may assume for simplicity that we are not now in the fixed angle region, so that the term $\sim |\bar{u}|^{-n} \ln |t|$ is not important. In the fixed angle region \mathcal{M}_2 will be small with respect to the Born term, anyhow.) The nonleading terms in \mathcal{M}_1 will generate important contributions to the sum; for instance, the term in $\mathcal{M}_1 \propto |\bar{u}|^{-n}$ will give a term in

$\mathcal{M}_2 \sim |u|^{-n} \ln |u|$ which will change $\alpha(t)$ and $\beta(t)$ as $|t|$ gets smaller and smaller.

However, the structure of the theory is most easily seen by considering only the biggest term in each order of the iteration.

The easiest way to see what will happen is to use the identity

$$\frac{1}{m!} |u|^{-n} \ln^m |u| = \frac{(-1)^m}{m!} \left. \frac{\partial^m}{\partial p^m} |u|^{-p} \right|_{p=n} \quad (3.35)$$

We can then insert a term $\propto (\bar{u} - \mu^2)^{-p}$ for \mathcal{M}_1 into the iteration equation which gives \mathcal{M}_2 , and at the end of the calculation differentiate with respect to p to reproduce the log factor. Before we differentiate, however, it will be convenient to calculate the Mellin transform of our expression and differentiate that with respect to p . We shall see that the left-most singularity is again a pole at $s = n$, but now it is a third order pole. Inverting the transform, this gives rise to a term $\propto |u|^{-n} \ln^2 |u|$.

To see in detail how this comes about, let us use (3.19b) to calculate the leading term of \mathcal{M}_2 . Using our well-known kernel and the first term on the right hand side of (3.33) for \mathcal{M}_1 , we find

$$\mathcal{M}_2 = \frac{\pi R_1(t) f^2(t) (-1)^n}{2(2\pi)^3} \left. \left(\frac{-\partial}{\partial p} \right) \frac{\Gamma(n+p)}{\Gamma(n)\Gamma(p)} I(u, t; p) \right|_{p=n} ; \quad |u| \rightarrow \infty \quad (3.36)$$

with

$$I(u, t; p) = \int_0^\infty dx dy d\alpha d\beta y^{n-1} x^{p-1} \delta(1-x-y-\alpha-\beta) \left[\mu^2 - \alpha \beta t - xyu \right]^{-(p+n)}$$

In deriving this form, we have again assumed that the masses of all external particles are zero, and the masses of all the internal particles are the same. For simplicity we have also used $(\bar{u} - \mu^2)$ as the argument of \mathcal{M}_1 instead of \bar{u} ,

but this doesn't affect the calculation of the leading terms. Now we want to double Mellin transform I as we did earlier in the calculation of \mathcal{M}_1 (3.28). This is easily done using the techniques described above, and we have

$$G(s, r; p) = 2\pi(\mu^2)^{s+r-p-n} \frac{\Gamma(s) \Gamma(r) \Gamma(p+n-s-r) \Gamma^2(1-r) \Gamma(n-s) \Gamma(p-s)}{\Gamma(p+n) \Gamma(2+n+p-2s-2r)} \quad (3.37)$$

which miraculously is the same as (3.30) for $p = n$. Now, taking the derivative of G with respect to p , and taking $p \rightarrow n$, we seek the left-most singularities in the s -plane in order to determine the asymptotic behavior of \mathcal{M}_2 for large $|u|$. Using the exciting properties of the well-known (! ?) poly-gamma functions,²⁶ it is easy to derive the formula for the leading singularities of the m^{th} derivative of the gamma function evaluated near zero:

$$\Gamma^{[m]}(x) = \frac{(-1)^m m!}{x^{m+1}} ; \quad x \rightarrow 0 \quad (3.38)$$

With this formula, we easily find that the left-most singularity of (3.37) in s is a sum of poles at $s = n$, the most singular of which is a third order pole. This comes from the term we get when we take the derivative of $\Gamma(p-s)$.

We invert this singularity using (3.27) and (3.32), and we find for the leading behavior of \mathcal{M}_2 as $|u| \rightarrow \infty$,

$$\mathcal{M}_2 = (-u)^{-n} \frac{f(t) R_1^2(t) \ln^2(-u)}{2!} . \quad (3.39)$$

It is easy to see from (3.38), (3.35) and (3.32), that if we continue this process keeping only the leading terms in each order, we will have the sum

$$\mathcal{M} = \sum_{j=0}^{\infty} \mathcal{M}_j = \frac{f(t)}{(-u)^n} \sum_{j=0}^{\infty} \frac{[R_1 \ln(-u)]^j}{j!} = f(t) (-u)^{R_1(t) - n} \quad (3.40)$$

And, as promised, the theory Reggeizes with $\alpha(t) = R_1(t) - n$ and $\beta(t) = f(t)$ in this approximation. There are of course other lower lying contributions in each order and these will enter the sum to change the behavior of α and β . We can see this already happening in (3.33) where the second term on the right "renormalizes" the residue, $\beta(t)$. In \mathcal{M}_2 , this term gets promoted and has a leading dependence $\propto (-u)^{-n} \ln(-u)$. This new term is just what is needed to allow the renormalized $\beta(t)$ to be simply factored out of the term $\propto \ln(-u)$ in the sum as we did in (3.40). It is clear that the number of lower lying terms which get promoted to modify α and β quickly proliferates, and makes a detailed prediction of the t -dependence of α and β for all t difficult. But it is equally clear that the structure of the theory is as shown in (3.40). In fact, since there is a coupling constant, say g , associated with each appearance of the kernel, (3.40) is exactly the perturbation result in the limit of small g — that is, to each order in $\ln(-u)$, (3.40) includes the minimum factors of g possible. It is also important to realize that regardless of the size of g , α and β are well approximated by

$$\begin{aligned} \alpha(t) &\simeq R_1(t) - n \\ &\quad (\text{large } |t|) \\ \beta(t) &\simeq f(t) \left[1 + R_0(t) \right] \end{aligned} \tag{3.41}$$

for large $|t|$. The reason is that as t increases $\mathcal{M}_{j+1} \ll \mathcal{M}_j$, and so at large $|t|$ it is certainly sufficient to consider only \mathcal{M}_0 and \mathcal{M}_1 .

Let us now return to (3.34). From this equation, we can see how the effective trajectory and residue approach their limits as t increases. For definiteness, we shall consider the case $n > 1$. If $n=1$, the discussion is similar. To examine the behavior of the trajectory we can expand (3.40) in powers of $\ln(-u)$ and compare with (3.34) (or, equivalently, use (3.41) and evaluate (3.34) for

large $|t|$). Doing this we find

$$\alpha(t) = \frac{B_1 f(t)}{(-t)} - n \quad (\text{large } |t|) \quad (3.42)$$

We see then that $\alpha(t)$ rises (or falls, depending on $f(t)$) away from its asymptotic value of $-n$ at a rate given by the first term in (3.42). In the BBG parton exchange model,²¹ n and the behavior of $f(t)$ are related to the electromagnetic form factors of the particles involved in the scattering, and so these form factors determine the rate at which the trajectory approaches its asymptote. Furthermore, this model also predicts that $f(t)$ has, at most a small imaginary part, and so in this order at least, $\alpha(t)$ is mostly real.

Another important aspect of the large $|t|$ behavior of our theory involves the definition of the deep scattering region. The deep region should be the region where coherent effects which build Regge poles become unimportant with respect to the Born term. Comparing (3.34) and the Born term, we see that the value of t where the deep region sets in depends upon u in the following way:

$$\frac{(-t)}{f(t)} \gtrsim \ln(-u)$$

In the BBG model, $f(t) \sim (-t)^{-b}$, where b is a small number (not necessarily an integer) whose order of magnitude is one, and depends on the specific reaction. The deep scattering region, therefore, is neither a fixed angle region ($t \propto u$) nor a fixed t region, but sets in someplace in between. In the more complicated coupled channel case, the relation which determines the deep region is generally somewhat more complicated, but the essential characteristic remains the same.

We promised the reader a few pages ago we would justify the use of, for example, the leading term of \mathcal{M}_1 in the calculation of \mathcal{M}_2 . To do this we must show that the most important region in the calculation of $\mathcal{M}_2(\mathcal{M}_{j+1})$

corresponds to large values of $|\bar{u}|$, the argument of $\mathcal{M}_1(\mathcal{M}_j)$ as $|u| \rightarrow \infty$. From (3.17), we see that since $0 < y < 1$ and $u < 0$, $|\bar{u}| \geq |yu|$ over the entire range of the ℓ_\perp integration, so it is sufficient to show that the important contributions come from regions when $|yu|$ is large. Now, let us look at the expression for I in (3.26). (We could just as well analyze (3.36), and the argument would be the same.) We may ask, for what values of the variables x and y is the integrand largest? By inspection (or differentiation with respect to $z \equiv xy$), we find that the integrand is largest when

$$xy|u| \sim \rho^2 + \alpha\beta|t| \quad (3.43)$$

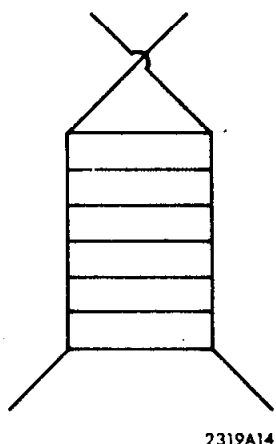
Since x , y , α and β are all between zero and one, the most stringent test of the size of \bar{u} will come when the right-hand side of this relation is finite. (It cannot be zero because of the term ρ^2 .) The relation $xy|u| = \text{constant}$ is a hyperbola in the $x - y$ plane. Remembering that $x, y \in [0, 1]$, we realize that over the entire length of the curve, except near one end point, $y|u| \rightarrow \infty$ as $|u| \rightarrow \infty$. The one region where this is not true is, of course, the segment which is very close to the point $x = 1$ where $y \sim \frac{1}{|u|}$. This segment shrinks to a point as $|u| \rightarrow \infty$. Since the integrand does not diverge here, it is safe to say that $|\bar{u}|$ is large in the most important region of integration in the recursion relation. Indeed, if the relation (3.43) is not satisfied, the integrand $\rightarrow 0$ as $|u| \rightarrow \infty$. The fact that derivatives with respect to p appear in higher order recursion relations such as (3.36) need cause no worry once it is realized that those derivatives are merely a convenient way of including the factors of logs which appear in the integrand. It is clear that the presence of these logs does not affect the validity of the argument presented here. Later in this section, we shall show that small values of $y(y \sim |u|^{-1/2})$ provide the most important contribution to the integral

as we approach the Regge region. In that case, it is a simple matter to show that the magnitude of energy variable appropriate to the kernel, $u' = (p-\ell)^2$, is also large in the region of interest. This is done by writing u' in terms of u , \bar{u} and y . This is, of course, required for a consistent theory. Finally, in section C, when we discuss the Reggeization problem in the coupled channel case, we shall refer again to our hyperbola, and show how the dominant region of integration determines how Reggeization takes place when the kernel does not have the same fall-off in u as the amplitude, \mathcal{M}_j , with which it is convoluted.

4. Discussion of the Kernel

It is instructive at this point to discuss the nature of the kernel and Born terms which appear in our integral equation. First, as we mentioned before, the blobs in Fig. (10) are supposed to be irreducible insertions in the two particle propagator. This, of course, is to avoid the problem of double counting of Feynman graphs. We would now like to examine a few simple examples of the insertions that can contribute to the kernel. In doing so we shall gain some insight into the role played by various s-channel and t-channel intermediate states in the theory.

In our discussion so far we have used a u-channel dispersion representation for K . Obviously, if we consider only simple ladder graphs (Fig. (14)) all of our results go through without complication and Reggeization proceeds apace. We can, of course, consider the same set of graphs by letting the kernel represent two horizontal propagators. Then, if we use the sum of a single propagator plus two simple propagators for the Born term we reproduce exactly the set of diagrams as represented in Fig. (14). (In the next subsection we shall use OFPT directly to derive our equation for these simple ladders.) It is important to realize that this can be done, since in the context of the parton interchange theory



2319A14

FIG. 14--Simple ladder graph.

of Gunion, Brodsky and Blankenbecler²¹ the kernels at large $|t|$ are box (or crossed box) diagrams with structure at the vertices, as in Fig. (15). The heavy lines here are hadrons, and the lighter, internal lines are quarks or cores. A proton, for example, may be thought of in this kinematic domain as a p quark plus a (pn) core or an n quark plus a (pp) core.

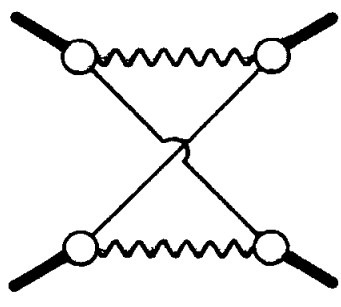
Motivated by these considerations, we want to look carefully in this section at the diagrams of Figs. (16) and (17). It is of course, important to consider these diagrams independent of any particular model, but if one subscribes to the parton interchange theory these diagrams are especially germane. Figure (16) is the type of graph which is expected to be important in building the vertex structure as in Fig. (15). Figure (17) on the other hand, corresponds to the insertion of an (su) graph into the kernel which is certainly present in some processes, especially in backward scattering according to Gunion, Brodsky and Blankenbecler.²¹ Let us turn first to a discussion of the vertex corrections, Fig. (16).

We proceed to calculate this graph by interpreting it as a Feynman graph (actually, a sum of Feynman graphs which include all relevant structures in the amplitude, $\bar{\mathcal{M}}$) and evaluating it in our now familiar infinite momentum frame. If we label the momenta as in Fig. (16), we can write this amplitude as

$$\mathcal{M} = \frac{1}{2(2\pi)^4} \int d^2 \ell_{\perp} \frac{dy}{|y|} d\ell^2 F(\ell^2, (p-\ell)^2) \bar{\mathcal{M}}(\bar{u}, t; \ell^2, (\ell+q)^2) \\ \left[(p-\ell)^2 - m^2 + i\epsilon \right]^{-1} \left[\ell^2 - m^2 + i\epsilon \right]^{-1} \left[(\ell+q)^2 - m^2 + i\epsilon \right]^{-1} \quad (3.44)$$

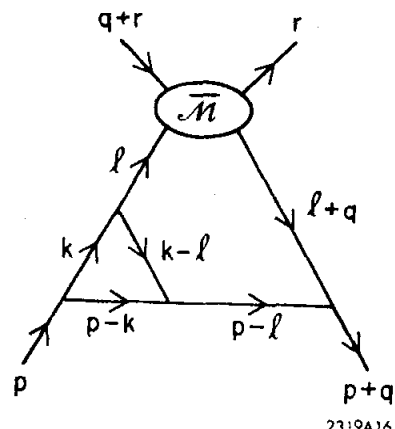
where the vertex function, F , is

$$F(\ell^2, (p-\ell)^2) = \frac{1}{2(2\pi)^4} \int d^2 k_{\perp} \frac{dz}{|z|} dk^2 \left[k^2 - m^2 + i\epsilon \right]^{-1} \left[(k-\ell)^2 - m^2 + i\epsilon \right]^{-1} \left[(p-k)^2 - m^2 + i\epsilon \right]^{-1} \quad (3.45)$$



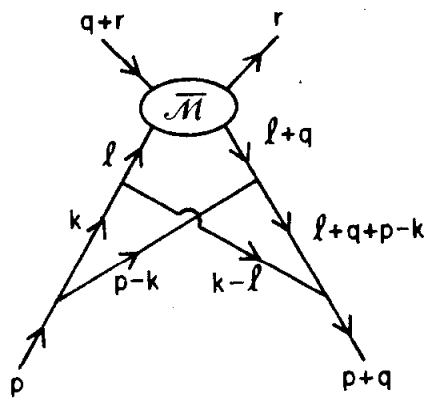
2319A15

FIG. 15--(tu) parton interchange diagram.



2319A16

FIG. 16--Feynman diagram showing kernel which includes a vertex correction.



2319A17

FIG. 17--Feynman diagram showing kernel which has a non-zero third double spectral function. (su-spectral function.)

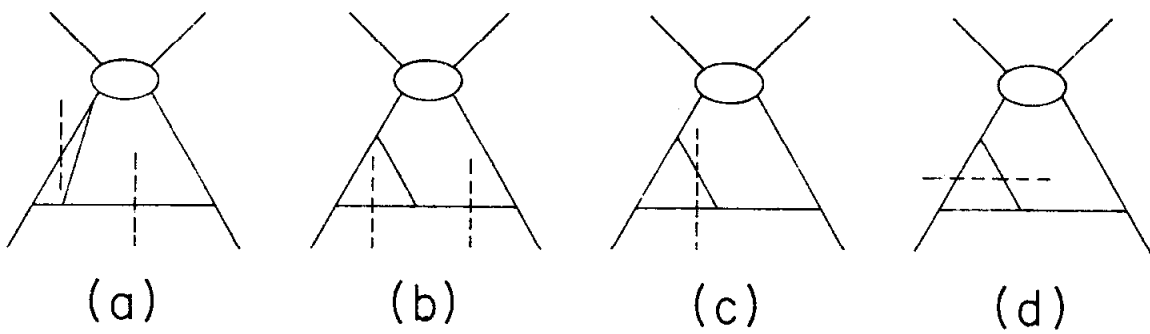
and our choice of frame dictates

$$k = \left(zP + \frac{k^2 + k_\perp^2}{2zP}, k_\perp, zP \right)$$

$$\ell = \left(xP + \frac{\ell^2 + \ell_\perp^2}{2yP}, \ell_\perp, yP \right)$$

For convenience, we have taken all masses equal.

We now want to do the dk^2 and $d\ell^2$ integrals. By arguments analogous to those presented in the derivation of our original equation we easily see that we get a non-zero contribution only when $z, y \in [0, 1]$. (Remember that r^2 and $(q+r)^2$ are spacelike.) Now let us imagine that we have used a spectral representation like (3.15) for $\bar{\mathcal{M}}$ in (3.44). As we discussed before, the weight function, \bar{W} , will not have any troublesome singularities in the ℓ^2 -plane. We may then analyze the positions of the singularities in ℓ^2 and k^2 by looking at the explicit propagators in (3.44). Then, at the end of the calculation we do the spectral integral over \bar{W} to get back $\bar{\mathcal{M}}$. With this procedure in mind, let us first suppose that $z < y$. Then, it is convenient to do the dk^2 integration by closing the contour in the lower half plane. Doing this we pick up a contribution from the pole at $k^2 = m^2 - i\epsilon$. (The other two poles are in the upper half plane.) We then perform the $d\ell^2$ integration closing the contour in the upper half ℓ^2 -plane. This picks up the pole at $(p-\ell)^2 - m^2 + i\epsilon = 0$. This contribution is shown in the time ordered graph of Fig. 18a) where the dashed lines indicate which particles are on the mass shell. Now, if $z > y$, we can close the k^2 contour in the upper half plane. For $z > y$ there is only one pole in this half plane, and we obtain a contribution from the pole at $(p-k)^2 - m^2 + i\epsilon = 0$. This time, when we do the $d\ell^2$ integral we find that we must consider contributions from two poles in the



2319A18

FIG. 18--Time orderings which contribute to the Feynman diagram Fig. 16 in the infinite momentum frame. The dashed lines show which intermediate state particles are on their mass shells.

ℓ^2 -plane. Closing the contour in the upper half plane, we get contributions from the poles at $(p-\ell)^2 - m^2 + i\epsilon = 0$ and $(\ell-k)^2 - m^2 + i\epsilon = 0$. These contributions are shown graphically in Figs. (18b) and (18c). (Remember, incidentally, that the propagator from the spectral representation of \bar{M} always has its pole in the lower half ℓ^2 -plane, and so we never surround this pole with our contour.)

The first point we want to comment on here is that all these contributions are contained in W in Eq. (3.11) with the cut in the σ^2 plane restricted to the positive real axis. Graphs (18a) and (18b) contribute to the pole at $\sigma^2 = m^2$, while (18c) gives the cut in W starting at $\sigma^2 = 4m^2$. Since these singularities are almost on the real axis, there is no reason to deform the $d\sigma^2$ contour from its usual choice. Another way of understanding this is to realize that there is no contribution like Fig. (18d) in this diagram. This means that the off mass shell variable, λ^2 , does not contribute any extra singularities of K in the ℓ^2 -plane which would introduce extra contributions to our integral equation had we not used the representation (3.11) for K . We emphasize again that these are two complementary ways of looking at the situation. If we do not introduce the dispersion representation (3.11) we, of course, need to calculate all the contributions of a specific graph, and some of them will, in general, be like Fig. (18d) (as we shall discuss shortly). However, once we introduce the dispersion relation (3.11) we can include all possible contribution from a general graph by keeping an open mind about the specific location of the $d\sigma^2$ contour. The appearance of extra off shell contributions like those in Fig. (18d) is equivalent to the requirement that the $d\sigma^2$ contour be deformed from the real axis to include complex singularities.²⁰ Therefore, as we stated before, our integral equation (3.20) or (3.21) is perfectly general with the understanding that the specific form of the $d\sigma^2$ contour depends upon W .

We would now like to describe what this vertex correction can tell us about the important s- and t-channel intermediate states in various kinematic regions. In subsection 3, we showed that in the integral equation the biggest contribution in the Regge limit came from a region near a hyperbola described by equation (3.43). We argued before that over most of this region, $|yu| \rightarrow \infty$ as $|u| \rightarrow \infty$. A glance at the expression for I in (3.26), however, also shows that the most important part of this hyperbola is the domain in which $x, y \rightarrow 0$ as $|u| \rightarrow \infty$. This is because the expression for I involves an integral over α and β , and, because of the δ -function, the allowed range of these integrals is maximized when x and y are both small. Therefore, the Regge region is dominated by the exchange of particles with small y .

We may now ask which of the vertex correction orderings we expect to dominate in the Regge region. Since small y is most important here, we expect the time orderings with $y < z$ will predominate. These are the graphs of Figs. (18b) and (18c). The picture of Regge behavior and its relation to deep scattering which emerges from these considerations is the following: the Regge region is dominated by the exchange of (light) particles with relatively small longitudinal momentum in the IMF (y near zero). If these particles are partons, we recover Feynman's idea that Regge behavior arises from the exchange of wee partons.²⁷ Notice, however, that the exchanged particles need not have point-like form factors or weird quantum numbers — our formalism includes the possibility that they are ordinary hadrons. Notice also that in generating Regge poles we only need to exchange two wee particles. However, the more complicated j -plane singularities that arise from s-channel iterations of simple poles will clearly correspond to amplitudes in which there are more than two wee particles exchanged. As we move away from the Regge region $|t|$ grows for fixed $|u|$, and,

as we see from (3.26), it becomes more and more important for α and β to be small in order to get a sizable contribution to I . Since the δ -function must be satisfied, regions of the y integration where y is not near zero become increasingly important, and it is no longer justifiable to consider only contributions to I coming from small y . As far as the vertex correction graphs are concerned this means that the time ordering of Fig. (18a) becomes more and more important. In addition, when $|t|$ is large all the amplitudes, \mathcal{M}_j , $j > 0$ are down by at least a factor $|t|^{-1}$ from the Born term, as we have shown. Hence, the picture in the s -channel is that in each amplitude, \mathcal{M}_j , the Regge region is dominated by the many particle intermediate states as in Figs. (18b and c) — whatever particles there are want to live as long as possible. In addition, amplitudes \mathcal{M}_j with increasingly large values of j become important in order to build up the moving Regge trajectory. As $|t|$ increases, each \mathcal{M}_j gets larger and larger contributions from diagrams like Fig. (18a) — that is, the particles in the intermediate state pull back and live for shorter and shorter times. Furthermore, as $|t|$ increases, all the amplitudes, \mathcal{M}_j for $j > 0$ become small in comparison with the Born term by at least a factor of $|t|^{-1}$, until finally in the deep region only the Born term is important. To complete the picture, we remark that a Born term should probably have a small number of intermediate state particles in order to be consistent with our interpretation. An example of such a Born term is provided by the parton interchange theory.²¹

Now let us turn to a brief discussion of the graph shown in Fig. (17). Our purpose here is to present an example of a kernel which, when used in our formulae, has singularities in ℓ^2 due to its dependence on Λ^2 , and which therefore requires a deformation of the path of integration in the σ^2 -plane. The specific kernel which we shall discuss has a non-zero third double spectral function (su),

and therefore is not really in the spirit of this section. This is because the on-shell amplitude corresponding to this kernel has discontinuities not only for positive u but for negative u also. Therefore, amplitudes built up from this kernel will not necessarily be real, and this is a complication which we wish to avoid for now, and relegate to section D. However, at the time of this writing, this reporter has not been able to think of a graph which has the disease we require, but which also has the discontinuities only for $u > 0$; hence, the present example. It is comforting to know, however, that for fixed t , $u \rightarrow \infty$, the leading term of this graph is not as big as the leading term of the graph with the horizontal rungs uncrossed.²⁸

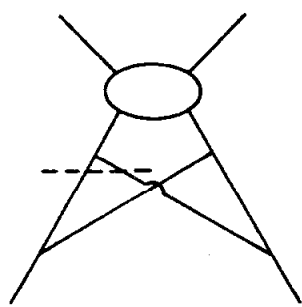
We proceed, then, with our analysis by labeling the momenta as in Fig. (17). Taking all masses equal, introducing a spectral representation for \mathcal{M} , and using the same frame as we used to discuss the vertex correction graph, we have for this diagram:

$$\mathcal{M} = \frac{1}{4(2\pi)^8} \int \frac{d^2 \ell \perp dy d^2 k \perp dz d\ell^2 dk^2}{|z| |y|} d\rho^2 \left[\ell^2 - m^2 + i\epsilon \right]^{-1} \left[(\ell+q)^2 - m^2 + i\epsilon \right]^{-1} \\ \left[k^2 - m^2 + i\epsilon \right]^{-1} \left[(\ell+q+p-k)^2 - m^2 + i\epsilon \right]^{-1} \left[(p-k)^2 - m^2 + i\epsilon \right]^{-1} \left[(k-\ell)^2 - m^2 + i\epsilon \right]^{-1} \\ \left[(\ell-r)^2 - \rho^2 + i\epsilon \right]^{-1} \bar{W}(\rho^2, t; \Lambda^2, R^2) \quad (3.46)$$

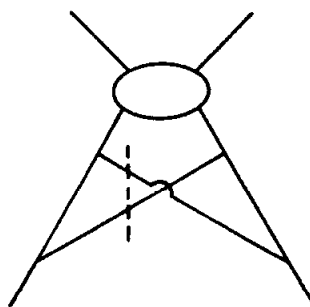
Examining the positions of the poles in ℓ^2 and k^2 , we discover that the only range of y and z which contribute in our frame is $0 < y < z < 1$. With this range of y and z , let us examine the dk^2 integral. It is straight forward to see that two of the four propagators which have poles in the k^2 -plane have their poles in the upper half plane, while the other two have poles in the lower half plane. We choose to close the contour in the lower half plane, and we thus pick up the poles from the propagators $\left[k^2 - m^2 + i\epsilon \right]^{-1}$ and $\left[(k-\ell)^2 - m^2 + i\epsilon \right]^{-1}$. We now carry out the $d\ell^2$

integral over the two contributions which result from these two poles. In the first term (obtained from the pole at $k^2 = m^2$) there are five poles in the ℓ^2 -plane, four of which are in the lower half plane (including the one from the spectral integral). Avoiding unnecessary emotional stress, we quietly close the $d\ell^2$ contour in the upper half plane, picking up a contribution from the propagator $[(k-\ell)^2 - m^2 + i\epsilon]^{-1}$. This contribution is shown graphically in Fig. (19a), where again the dashed lines denote which internal particles are on the mass shell. A similar analysis for the second term again reveals that four of the five poles in ℓ^2 are in the lower half plane. Closing the contour in the upper half ℓ^2 -plane, we pick up a contribution from the pole generated by the propagator $[(p-k)^2 - m^2 + i\epsilon]^{-1}$. This term is shown in Fig. (19b).

We can now clearly see the kinds of terms which require a deformation of the spectral integral contour. Figure (19a) represents a contribution to the amplitude in which λ^2 has gotten sufficiently time-like to decay freely into the two particles which are on the mass shell, and therefore requires the existence of complex singularities in the σ^2 -plane. Figure (19b), on the other hand, is just an ordinary contribution of the type we have seen before, and by itself could be treated by a path integration running along the real σ^2 -axis. Notice that if we were interested in only the imaginary part of this diagram (for instance, if the top two external masses were photons and we were calculating W_1 or νW_2), only the contribution (19b) would be relevant. The reason is that all the intermediate state particles are required to be on-shell for the imaginary part, and this cannot be the case for Fig. (19a). To put it more graphically, only (20b) and not (20a) contributes to the imaginary part of the full amplitude, since (20a) represents a discontinuity in the mass $(q+r)^2$ and not in $s = (p+q+r)^2$. This analysis successfully accounts for Polkinghorne's observation that in the



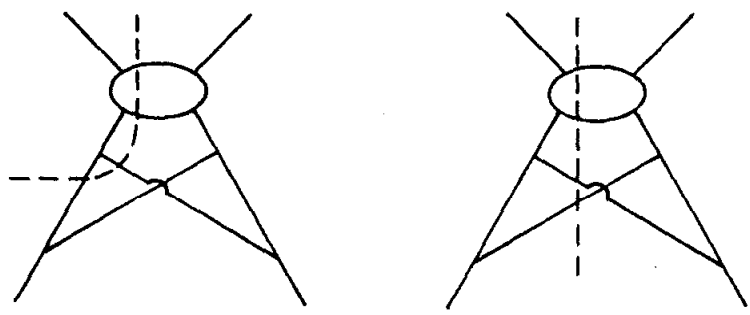
(a)



(b)

2319A19

FIG. 19--Contributions to Fig. 17. The intermediate state particles that are on mass-shell are indicated by the dashed lines.



(a)

(b)

2319A20

FIG. 20--Possible contributions to the imaginary part
of the Feynman diagram, Fig. 17. Figure 20a
does not contribute for stable external particles.

covariant parton model calculation of νW_2 the off-shell parton leg is space-like.²⁹

However, our discussion shows that this would not, in general, be true if one undertook a calculation of the complete Compton amplitude.

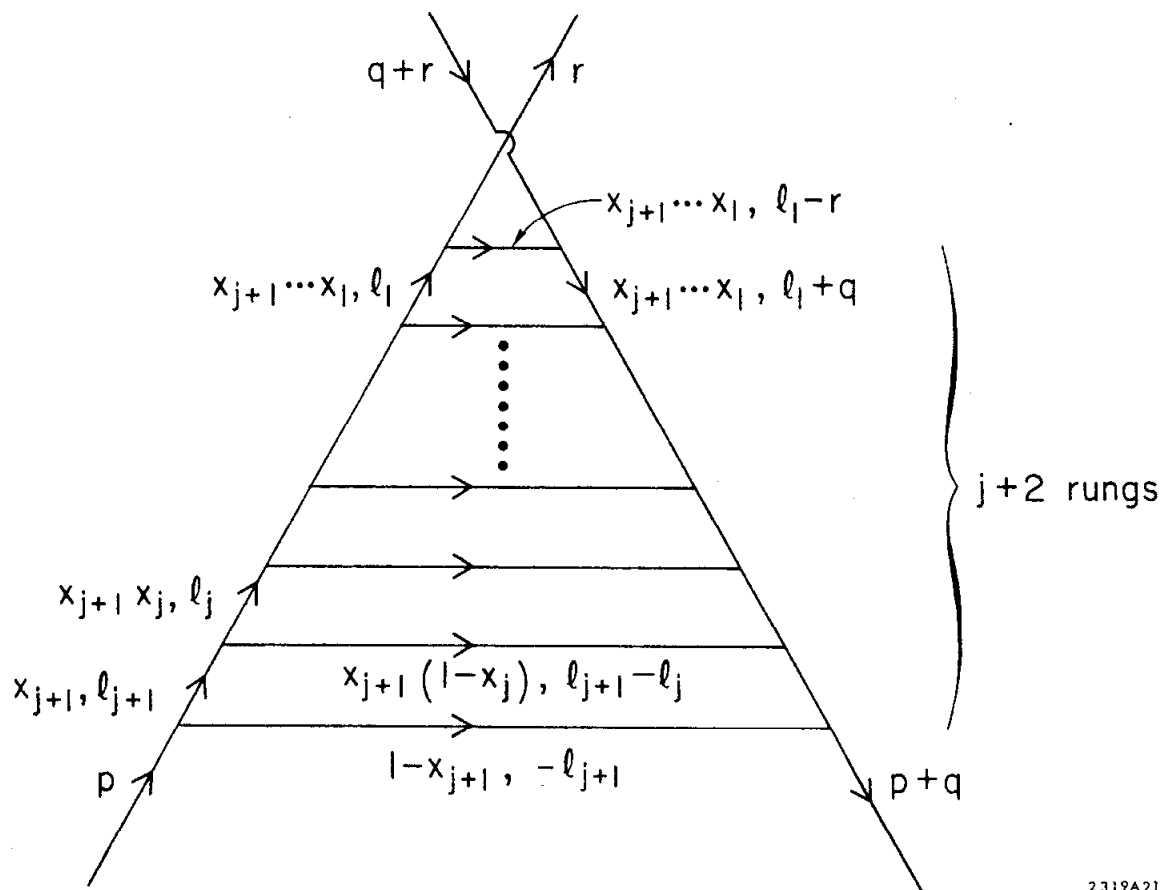
By carefully examining two Feynman graphs which can contribute to K , we have tried in this subsection to gain a better understanding of the physical interpretation, as well as the mathematical complexities, of our Reggeization procedure. We now want to return to the simplest realization of our theory — the basic ladder graphs. We present, in the next subsection, an alternate derivation of our integral equation for this case.

5. Alternate Derivation Using OFPT

To conclude this rather lengthy section then, let us proceed to outline the derivation of our basic integral equation, (3.20) or (3.21), using old-fashioned perturbation theory in the infinite momentum frame directly. This derivation is somewhat more cumbersome than the one presented in subsection 2, and the extent to which the final equation is model independent is not readily apparent. Nevertheless, it is interesting to see how the equation emerges from this approach. For simplicity, we shall only treat the case of simple ladder graphs, but it will be apparent that the procedure applies also to more complicated cases.

Let us begin by turning to Fig. (21). This figure represents the amplitude \mathcal{M}_{j+1} and consists of $j + 2$ rungs (one from the Born term). As in subsection 2, we choose our frame and external momenta such that $(q+r)^2$ and r^2 are space-like. We consider the limit $P \rightarrow \infty$ and parameterize the external momenta as

$$\begin{aligned} p &= \left(P + \frac{\nu^2}{2P}, 0, P \right) \\ q &= \left(\frac{q \cdot p}{P}, q_\perp, 0 \right) \\ r &= \left(\frac{r \cdot p}{P}, r_\perp, 0 \right) \end{aligned}$$



2319A21

FIG. 21--Only surviving time ordering for the old-fashioned perturbation theory calculation of simple ladder graphs.

and we assume that the final state particle with momentum $(p+q)$ has a mass ν'^2 .

The parameterizations of the internal momenta are indicated in Fig. (21). The factors of x_i represent the fraction of longitudinal momentum carried by that line, and the ℓ_i (or $\ell_i + q_\perp$ or $\ell_1 - r_\perp$) are the transverse momenta carried by the line.

According to the OFPT rules given in subsection 1, we conserve 3 momentum at each vertex and place all the particles on their mass shells. The momentum vectors of all the internal lines are then easily written down. For example, the four-vector of the second from the bottom rung of the ladder is

$$\left(x_{j+1}(1-x_j) P + \frac{m^2 + (\ell_{j+1} - \ell_j)^2}{2x_{j+1}(1-x_j)P}, \ell_{j+1} - \ell_j, x_{j+1}(1-x_j) P \right)$$

For simplicity, we set the mass of each internal line equal to m .

With this parameterization of momenta, the only time ordering that survives in the $P \rightarrow \infty$ limit is the one shown in Fig. (21) which we now read as a time-ordered, rather than a Feynman diagram with time running from left to right. The fractions x_i are all between 0 and 1 so that the z-component of momentum is positive for each internal line. To calculate the graph, we need expressions for the energy denominators according to the rules of subsection 1. On the left side of the graph, we label the energy denominators by defining $2P$ times the energy difference to be D_i with i running from 1 to $j+1$. D_{j+1} is calculated from the intermediate state which appears after the first vertex and D_1 refers to the intermediate state just to the left of center (the so-called liberal state). Similarly, the energy denominators (times $2P$) calculated from the right side of the graph are labeled by E_i . $2P$ times the central energy denominator we shall call Δ . If the coupling constant at the vertices is g , we can easily write down an

expression for the amplitude. It is

$$M_{j+1}(u, t; N^2, R^2) = \left(\frac{g^2}{2(2\pi)^3} \right)^{j+2} \int \prod_{i=1}^{j+1} \left\{ \frac{d^2 \ell_i dx_i}{(x_i)^{1+2i} (1-x_i) D_i E_i} \right\} \Delta^{-1} \quad (3.47)$$

It is convenient to represent the D_i and E_i by a sum of energy differences across each vertex. Doing this we easily find

$$D_{j+1} = \nu^2 - S(\ell_{j+1}, x_{j+1})$$

$$D_i = D_{j+1} + \sum_{k=i}^j \frac{1}{w_{k+1}} \left[m^2 - S(\ell_k - x_k \ell_{k+1}, x_k) \right] \quad j \geq i \geq 1$$

$$E_{j+1} = \nu'^2 - S(\ell_{j+1} + (1-x_{j+1}) q_\perp, x_{j+1})$$

$$E_i = E_{j+1} + \sum_{k=i}^j \frac{1}{w_{k+1}} \left[m^2 - S(\ell_k - x_k \ell_{k+1} + (1-x_k) q_\perp, x_k) \right] \quad j \geq i \geq 1 \quad (3.48)$$

where

$$w_k = x_{j+1} x_j \cdots x_k$$

and

$$S(\ell, x) = \frac{\ell^2 + m^2}{x(1-x)}$$

S is, of course, the same kind of variable that appears in (3.6) as well as subsequent formulae. Finally, we can write Δ in the form

$$\Delta = D_1 + u + r_\perp^2 - \nu^2 + \frac{1}{w_1} \left[\ell_1^2 - (\ell_1 - r_\perp)^2 \right] \quad (3.49)$$

Now, since the $d^2\ell$, integrations cover an entire plane we are free to shift the origin of each integration. Therefore, define a new set of transverse vectors by

$$\ell'_j = \ell_j + x_j \ell_{j+1}$$

and

$$\ell'_i - x_i \ell'_{i+1} = \ell_i - x_i \ell_{i+1} \quad (3.50)$$

With this transformation, we can write

$$x_{j+1} D_i = \bar{D}_j + \sum_{k=i}^{j-1} \frac{1}{\bar{w}_{k+1}} \left[m^2 - S(\ell'_k - x_k \ell'_{k+1}, x_k) \right] \quad j \geq i \geq 1 \quad (3.51)$$

where

$$\bar{D}_j \equiv \lambda^2 - S(\ell'_j, x_j)$$

with

$$\lambda^2 = x_{j+1} \nu^2 - \frac{\ell'_{j+1}^2 + x_{j+1} m^2}{1 - x_{j+1}}$$

and

$$x_{j+1} \bar{w}_{k+1} = w_{k+1}$$

λ^2 as defined here is exactly the off-mass shell variable defined in (3.17) with $\sigma^2 = m^2$ and is the square of the four momentum flowing up the left side of the ladder just after the first vertex in Fig. (21). Now, notice that the right hand side of (3.51) is exactly what we would get for D_i if we were to calculate the amplitude \mathcal{M}_j (instead of \mathcal{M}_{j+1}) with an incoming mass λ^2 rather than ν^2 . The transformation (3.50) also allows us to rewrite $x_{j+1} E_i$ in a way similar to (3.51)

only with the replacement

$$\nu'^2 \rightarrow \lambda'^2 = x_{j+1} \nu'^2 - \frac{(\ell_{j+1} + (1-x_{j+1})q_{\perp})^2 + x_{j+1} m^2}{1 - x_{j+1}}$$

As before, this is the same as λ'^2 as defined in (3.17) (with $\sigma^2 = m^2$) and has an interpretation similar to the interpretation of λ^2 . Finally, using (3.50) we can write for the central energy denominator

$$x_{j+1} \Delta = x_{j+1} D_1 + \bar{u} + r_{\perp}^2 - \lambda^2 + \frac{1}{w_1} \left[\ell_1^2 - (\ell_1^2 - r_{\perp}^2)^2 \right] \quad (3.52)$$

where

$$\bar{u} = x_{j+1} u - \frac{(\ell_{j+1} + (1-x_{j+1})r_{\perp})^2 - x_{j+1} m^2}{1 - x_{j+1}}$$

and, again, with $\sigma^2 = m^2$ is the variable defined in (3.17). Using (3.51), and comparing (3.49) with the right hand side of (3.52), we recognize this as the central energy denominator calculated for the amplitude \mathcal{M}_j with $\nu^2 \rightarrow \lambda^2$ and $u \rightarrow \bar{u}$. Therefore, if we define $\ell = \ell_{j+1}$, and $y = x_{j+1}$, we may rewrite (3.47) as

$$\mathcal{M}_{j+1}(u, t; N^2, R^2) = \frac{g^2}{2(2\pi)^3} \int \frac{d^2 \ell dy}{y^2(1-y) D_{j+1} E_{j+1}} \mathcal{M}_j(\bar{u}, t; \Lambda^2, R^2) \quad (3.53)$$

Using the definitions of D_{j+1} and E_{j+1} (3.48), we easily see that (3.53) is a special case of (3.19b) with

$$W(\sigma^2, t; N^2, \Lambda^2) = \delta(m^2 - \sigma^2)$$

as befits a kernel which consists of a simple pole at m^2 . To complete the OFPT

derivation of the integral equation, we need only sum both sides of (3.53) over j , and we will have reproduced (3.21) for the case of the simple ladder graphs.

This procedure is clearly valid for a large class of kernels and in general will reproduce the integral equation derived in subsection 2. An interesting property of the OFPT derivation is that it provides yet another example of how clever Feynman diagrams are. Consider, for example, an OFPT derivation in which the kernel consists of the bottom two rungs of a ladder graph. In our usual frame, only one time ordering of the four vertices of this kernel will contribute (as in Fig. (21)). After calculating the diagram we are free to introduce a dispersion representation for the kernel. Strictly speaking, however, the weight function, W , which we should use for this kernel is not the weight function for the entire covariant sub-amplitude (with off-shell masses), but is the weight function appropriate to the single contributing time ordering. It is a testimony to the ingenuity of our integral equation that it automatically projects out the relevant piece of the weight function so that it is allowable to insert a spectral representation for the complete covariant sub-amplitude. Of course, in the context of the derivation of subsection 2, this property is obvious, so maybe the lesson to be learned here is that there is often a great advantage in keeping expressions covariant as long as possible.

In this section we have tried to indicate by a simple example, the connection between two alternate derivations of Eqs. (3.20) and (3.21). While the present derivation is not as simple and not as obviously general, it does cast the problem in a slightly different way, and so is useful in that respect.

C. The Coupled Channel Case

In the last section, we discussed at some length the problem of Reggeizing deep scattering in a world where there is only one kind of particle whose deep

elastic amplitude has only a right hand cut in u . (This is almost equivalent, in our case, to saying that there is only one nonzero double spectral function $(t-u)$.) While this discussion yielded much physical insight, there are at least two additional layers of complexity that must be added in order to make reasonable contact with the hadronic world. First, it is well known that there is more than one kind of strongly interacting particle, and so a realistic theory must incorporate this feature of high energy phenomenology. Second, it has long been suspected that crossing symmetry and direct-channel unitarity may be important in hadron physics, and that would seem to imply the necessity of at least considering the existence of discontinuities at negative, as well as positive u . In this section we shall deal with the first of these complications and in the next section we shall discuss the second. (We shall, however, continue to work only with spinless particles.)

The inclusion of more than one particle actually involves two kinds of generalizations. Consider, for example, a world of N particles. If we restrict ourselves to a discussion only of elastic scattering in the s -channel, we need to incorporate N^2 coupled amplitudes into our formalism. Some sort of matrix method suggests itself, and that is what we shall discuss later in this section. In addition, however, we must now consider the problem of how Reggeization takes place when we convolute two sub-amplitudes which have different power law behaviors in u . This is the problem to which we turn first. We shall, of course, still continue to use kernels and Born terms which have discontinuities for positive u only.

Suppose, therefore, that we wish to convolute an amplitude, \bar{M} , whose asymptotic behavior for large $|u|$ is given by

$$\bar{M} = h(t) (\mu^2 - u)^{-m} \ln^k (\mu^2 - u) = h(t) \left(\frac{-\partial}{\partial m} \right)^k (\mu^2 - u)^{-m} \quad (3.54)$$

with a kernel, K , whose asymptotic form is

$$K = f(t) (\mu^2 - u)^{-n} \quad (3.55)$$

in our integral equation (recursion relation) (3.19b). For convenience, we take m, n and k to be integers. We may use (3.12) which is the imaginary part of K in (3.19b), and we have

$$\begin{aligned} \tilde{\mathcal{M}} = & \frac{f(t) h(t)}{2(2\pi)^3 (n-1)!} \left(\frac{-\partial}{\partial m} \right)^k \int_0^1 dy \frac{d^2 \ell_{\perp} d\sigma^2}{y^2 (1-y)} \left[\nu^2 - S(\ell_{\perp}, y) \right]^{-1} \\ & \left[\nu^2 - S(\ell_{\perp} + (1-y) q_{\perp}, y) \right]^{-1} \delta^{[n-1]} (\mu^2 - \sigma^2) (\mu^2 - u)^{-m} \end{aligned} \quad (3.56)$$

Using the identity above (3.25), as well as (3.17), we easily derive the analogue of (3.25) for our present case:

$$\begin{aligned} \tilde{\mathcal{M}} = & \frac{f(t) h(t)}{2(2\pi)^3 (n-1)!} \left(\frac{-\partial}{\partial m} \right)^k m(m+1) \int_0^1 dy (1-y)^{m+1} d^2 \ell_{\perp} d\sigma^2 \\ & \delta^{[n-1]} (\mu^2 - \sigma^2) d\alpha_1 d\alpha_2 d\alpha_3 \delta(1-\alpha_1 - \alpha_2 - \alpha_3) \alpha_3^{m-1} \\ & \times \left[\rho'^2 + \ell_{\perp}^2 + (1-y)^2 \alpha_1 \alpha_2 q_{\perp}^2 - y(1-y) \alpha_3 u + y \sigma^2 \right]^{-(m+2)} \end{aligned} \quad (3.57)$$

with ρ'^2 defined as in (3.25). The $d^2 \ell_{\perp}$ and $d\sigma^2$ integrals are done just as they were in section B, and we find for the present case

$$\tilde{\mathcal{M}} = \frac{\pi f(t) h(t) (-1)^n}{2(2\pi)^3} \left(\frac{-\partial}{\partial m} \right)^k \frac{\Gamma(n+m)}{\Gamma(n) \Gamma(m)} I(u, t) \quad (3.58)$$

where

$$I(u, t) = \int_0^{\infty} dx dy d\alpha d\beta \delta(1-x-y-\alpha-\beta) x^{m-1} y^{n-1} \left[\rho^2 - \alpha \beta t - xyu \right]^{-(m+n)}$$

and, as before, we have defined $x = (1-y)\alpha_3$, $\alpha = (1-y)\alpha_1$, $\beta = (1-y)\alpha_2$, and $\rho^2 = \rho'^2 + y\mu^2$.

We now want to examine the leading terms of \tilde{M} for large $|u|$. We do this, not surprisingly, by again using Mellin transforms. The double Mellin transform of I defined in (3.28) is easily calculated. In fact, we have already done this in (3.37) when we were examining the behavior of the second iterated matrix element, M_2 , in the last section. For ease of calculation, we again set all the external masses equal to zero and all the internal masses equal to μ . Then, we easily verify,

$$G(s, r) = 2\pi(\mu)^{2s+r-m-n} \frac{\Gamma(s)\Gamma(r)\Gamma(m+n-s-r)\Gamma^2(1-r)\Gamma(n-s)\Gamma(m-s)}{\Gamma(m+n)\Gamma(2+m+n-2s-2r)} \quad (3.59)$$

which is the same as (3.37) with $p = m$. With this formula, we can clearly examine the asymptotic behavior of \tilde{M} in $|u|$ for all values of t , in particular in both the limits $\frac{t}{u} \rightarrow 0$ and $\frac{t}{u}$ fixed as $|u| \rightarrow \infty$. Since we have already done this for the problem of the last section, we will only consider the $\frac{t}{u} \rightarrow 0$ limit here. That will be sufficient for the physical point we wish to make.

To examine the large $|u|$ behavior of (3.58), in this limit, we put r near zero (but positive) and look in the s -plane, analyzing the singularities of G for positive s . The three cases to consider are $n = m$, $n > m$, and $n < m$. For the physical reasons discussed in the last section, we assume that $n, m \geq 1$. Now, if $n = m$ we have exactly the situation of section B. To review, in this case the first singularity which we run across in s is a pole at $s = m$. By applying the derivative $\frac{-\partial}{\partial m}$ to $\Gamma(m-s)$ k times, we generate a $(k+1)^{\text{th}}$ order pole at $s = m$. But, since $n = m$ the factor $\Gamma(n-s)$ contributes another order to this pole, and we end up with a pole at $s = m = n$ of order $k+2$. Mellin inverting this singularity

tells us that the leading behavior of \tilde{M} is

$$\tilde{M} \sim (-u)^{-m} \ln^{k+1}(-u); \quad (n=m) \quad (3.60)$$

and the theory Reggeizes, as discussed in detail in the last section.

It is easy to see what happens if $n \neq m$. For $n < m$, the first singularity in s is a simple pole at $s = n$, and the leading behavior of \tilde{M} is given by

$$\tilde{M} \sim (-u)^{-n}; \quad (n < m) . \quad (3.61)$$

On the other hand, if $m < n$, we have, after applying the derivatives $\left(\frac{-\partial}{\partial m}\right)^k$ to $\Gamma(m-s)$ a pole of order $(k+1)$ at $s = m$. Since this is now the first singularity of G in the s -plane for positive s , we have the asymptotic dependence,

$$\tilde{M} \sim (-u)^{-m} \ln^k(-u); \quad (m < n) . \quad (3.62)$$

Of course, in both the cases with $n \neq m$ there are lower lying terms of the form (3.61) or (3.62), and the sum of these terms must approach (3.60) as $n \rightarrow m$.

What is the physical interpretation of this result? Evidently, when $n \neq m$, the amplitude \tilde{M} does not seem to know that it is supposed to represent the convolution of two sub-amplitudes, at least as far as the leading term is concerned. If $n > m$ ($n < m$), the asymptotic behavior of \tilde{M} is the same as the asymptotic behavior of \tilde{M} (K). Physically, the reason is that the faster the fall-off of the sub-amplitude, the more the z -component of momentum wants to flow through the other sub-amplitude. The momentum, therefore does not sample this sub-amplitude, and the leading behavior of \tilde{M} does not reflect its behavior. As the sub-amplitude falls off faster and faster it behaves more and more like an open circuit and shunts the momentum through the other rung.

We can understand this result from the following point of view. In the last section, we showed that the major contribution to our integral in the $|u| \rightarrow \infty$ limit comes for the region near a hyperbola $xy|u| = \text{const.}$ Looking at the expression for I in (3.58), it is easy to see how the delicate balance in the flow of momentum which produces a log by allowing y to sample both amplitudes is upset when $m \neq n$. When $n > m$ ($n < m$), the integral prefers larger (smaller) values of y , thus destroying the symmetry in x and y and shifting the dominant region of integration away from the symmetry point of the hyperbola ($x, y \sim |u|^{-1/2}$) toward larger (smaller) values of y . (Remember, that because of the form of the integral, when y samples both sub-amplitudes it is small $\sim |u|^{-1/2}$, and not $\sim \frac{1}{2}$.)

Although we do not gain extra log factors when $n \neq m$, we must include such graphs in the calculation of the final Reggeized amplitude. Since, in a realistic case we will continue to generate amplitudes, \mathcal{M}_j , ad infinitum, with all possible combinations of kernels, the terms generated in a situation where $n \neq m$ will eventually Reggeize, and will contribute to $\alpha(t)$ and $\beta(t)$ higher order terms in the couplings associated with the kernels.

Fortified by this discussion, we now face the task of developing the formalism necessary to handle problems with more than one kind of particle. The most convenient way to do this is to discuss in detail an example with two particles. Our example will be of complexity sufficient to reveal all the salient physical features, and the extension to the most general case will be obvious.

Consider then, a world with two kinds of particles, 1 and 2. Since we limit our discussion to s-channel elastic amplitudes, we need to consider a total of four amplitudes, $\mathcal{M}^{\alpha\beta}$. The superscripts refer to the particles in the t-channel. The first superscript refers to the type of particle coming our of the bottom of the

amplitude, and the second superscript refers to the particles coming out of the top. Thus, \mathcal{M}^{21} is the amplitude for the s-channel process $1+2 \rightarrow 1+2$, etc.

Notice that $\mathcal{M}^{\alpha\beta}$ is symmetric. For simplicity, we shall not discuss backward scattering in this section, but our formalism could easily be generalized to include it.

The particular example we want to consider is defined by specifying the Born terms which we also choose to be the kernels. They will be given by:

$$K^{\alpha\beta} = B^{\alpha\beta} = f^{\alpha\beta}(t)(\mu^2 - u)^{-n} + h^{\alpha\beta}(t)(\mu^2 - u)^{-m}. \quad (3.63)$$

With the definition of the weight function as in (3.11), we have

$$W^{\alpha\beta} = \frac{f^{\alpha\beta}(t)}{(n-1)!} \delta^{[n-1]}(\sigma^2 - \mu^2) + \frac{h^{\alpha\beta}(t)}{(m-1)!} \delta^{[m-1]}(\sigma^2 - \mu^2) \quad (3.64)$$

One particular case of physical interest corresponds to the choice $f^{22} = h^{12} = h^{21} = h^{11} = 0$. The rest of the Born matrix elements are non-zero, and $m > n$. If particle 1 is a k^+ and 2 is a p , this example corresponds in the parton interchange theory to the case of $k^+ - p$ coupled channels. The reason why we choose $k^+ - p$ is that all four s-channel amplitudes are exotic, and we expect only (tu) graphs to contribute, leading to purely real amplitudes. Of course, in the real world, we must include other intermediate states, also, such as pions. This will have the effect of introducing imaginary parts to the purely real amplitudes which we will generate in present problem, and should help to build up a pomeron pole. This will be discussed further in the next section.

Using the kernel given in (3.63), let us calculate the second order matrix element, $\mathcal{M}_1^{\alpha\beta}$. For a given set of external particles, we must include contributions when the t-channel intermediate state contains particles either of type 1 or

of type 2. Using our standard recursion relation (3.19a), we may therefore write,

$$\mathcal{M}_1^{\alpha\beta}(u, t; N^2, R^2) = \frac{1}{2(2\pi)^3} \sum_{\gamma=1}^2 \int_0^1 \frac{dy d^2\ell}{(1-y)} \left[\lambda^2 - m_\gamma^2 + i\epsilon \right]^{-1} \left[\lambda^2 - m_\gamma^2 + i\epsilon \right]^{-1} \\ w^{\alpha\beta}(\sigma^2, t; N^2, \Lambda^2) \mathcal{M}_0^{\gamma\beta}(\bar{u}, t; \Lambda^2, R^2) \quad (3.65)$$

Where m_γ is the mass of the γ^{th} particle. Since we have two kinds of Born terms, we have a total of four contributions coming from (3.65), each one of which, in general, contributes to each of the four amplitudes under discussion. From the previous discussions of the section, and from (3.58), it is clear that each of these four terms can be written

$$\sum_{\gamma} \frac{\pi(-1)^a \Gamma(a+b)}{2(2\pi)^3 \Gamma(a) \Gamma(b)} g_b^{\alpha\gamma}(t) g_a^{\gamma\beta}(t) I(u, t; a, b, \gamma) \quad (3.66)$$

with

$$I(u, t; a, b, \gamma) = \int_0^\infty dx dy d\alpha d\beta \delta(1-x-y-\alpha-\beta) x^{a-1} y^{b-1} \left[\rho^2 - \alpha\beta t - xyu \right]^{-(a+b)}$$

ρ^2 is as defined below (3.58), but with $m^2 \rightarrow m_\gamma^2$. Furthermore, it is understood that at the end of the calculation, one continues the external masses ν^2 , $\nu'^2 \rightarrow m_\alpha^2$, and $r^2, (q+r)^2 \rightarrow m_\beta^2$. With the Born terms and kernel given by (3.63), a and b can take on the values m or n , and $g_n = f$ and $g_m = h$.

We first wish to examine the term $\propto [f(t)]^2$ ($a = b = n$). Therefore, let us now consider a problem with only one variety of Born term, and set $h^{\alpha\beta} = 0$. The u -dependence arising from \mathcal{M}_1 for such a problem has been discussed in exhausting detail in the last section. We know that for large $|u|$, $\mathcal{M}_1 \propto (-u)^{-n} \ln(-u)$. In this limit we may therefore write the matrix elements to second order in the

couplings as

$$\mathcal{M}^{\alpha\beta} = f^{\alpha\beta}(t)(\mu^2 - u)^{-n} + \sum_{\gamma} f^{\alpha\gamma}(t)f^{\gamma\beta}(t) H(t; \gamma)(\mu^2 - u)^{-n} \ln(\mu^2 - u) \quad (3.67)$$

where $H(t; \gamma)$ is the coefficient of $f^2(-u)^{-n} \ln(-u)$ with t-channel intermediate state particles of mass m_{γ} . H may be exactly calculated from (3.66) using Mellin transform techniques or, may be evaluated using the formulae following (3.36). In any case, it is useful to recall that (mod logs) $H(t) \sim t^{-1}$ for large $|t|$.

Now, can we make anything simple out of (3.67)? Before answering that question, we should remember that whatever solution we finally reach for our problem, it should incorporate the property of factorization of the Regge residues. This factorization is to be contrasted with the lack of factorization in the Born terms. There is no reason to suppose that just because, say $f^{22}=0$, $f^{12}=0$ also. (In fact, the example we referred to earlier had $f^{22}=0$, $f^{12} \neq 0$.) Now, if we tried to represent (3.67) with a single Regge pole, we would not be able to achieve the factorization property, in the residue since $\beta_+^{\alpha\beta}(t) \rightarrow f^{\alpha\beta}(t)$ for large $|t|$. It is therefore necessary to introduce at least two trajectories which have $\alpha(t) \rightarrow -n$ as $|t| \rightarrow \infty$. If we write

$$\mathcal{M}^{\alpha\beta} = \beta_+^{\alpha\beta}(t)(-u)^{\alpha_+(t)} + \beta_-^{\alpha\beta}(t)(-u)^{\alpha_-(t)}, \quad (3.68)$$

we can expand

$$(-u)^{\alpha(t)} = (-u)^{-n} e^{(\alpha+n)\ln(-u)} \cong (-u)^{-n} (1 + (\alpha+n)\ln(-u))$$

for α near $-n$, and identify terms in like powers of $\ln(-u)$ in (3.67) and (3.68).

Doing this we find

$$f^{\alpha\beta}(t) = \beta_+^{\alpha\beta}(t) + \beta_-^{\alpha\beta}(t) \quad (3.69)$$

and

$$f^{\alpha\gamma}(t) H^{\gamma\delta}(t) f^{\delta\beta}(t) = (\alpha_+(t) + n) \beta_+^{\alpha\beta}(t) + (\alpha_-(t) + n) \beta_-^{\alpha\beta}(t)$$

where we now consider the scalar function H to be a diagonal matrix, and matrix multiplication is implied on the left of the second equation. In addition to these equations, we have the factorization conditions on each of the residues:

$$\beta_{\pm}^{11}(t) \beta_{\pm}^{22}(t) = (\beta_{\pm}^{12}(t))^2 \quad (3.70)$$

which in our simple case of only two coupled channels can be written as

$$\text{Det}[\beta_{\pm}(t)] = 0.$$

Expressions (3.69) and (3.70) comprise a set of ten bilinear equations in the ten unknowns, $\alpha_{\pm}(t)$ and $\beta_{\pm}^{\alpha\beta}(t)$. (Because of the symmetry requirements of the matrices, however, there are really only eight independent equations and eight unknowns.) Since the equations are symmetric under the interchange $(+ \leftrightarrow -)$, these equations uniquely determine the unknowns up to the arbitrary assignment of the (\pm) labels.

To solve these equations conveniently, one can rewrite the second of Eqs. (3.69) by subtracting $(\alpha_+ + n)\beta_-$ from both sides. Pulling the term $(\alpha_+ + n)\beta_+$ to the left side, and then taking the determinant of both sides we find

$$\text{Det} [fHf - (\alpha_{\pm}(t) + n)f] = 0 \quad (3.71)$$

where we have used the first of Eqs. (3.69), as well as (3.70). Notice that (3.71) holds for $\alpha_-(t)$ as well as $\alpha_+(t)$ because of the (\pm) symmetry of the problem. Hence, (3.71) is a second degree equation in the α 's and determines the eigen trajectories of our problem to this order in the couplings. The solutions are easily found, and can be conveniently expressed in the following form:

$$\alpha_{\pm}(t) + n = \frac{1}{2} \left(\text{Tr}[fH] \pm \left[(\text{Tr}[fH])^2 - 4 \text{Det}[fH] \right]^{1/2} \right). \quad (3.72)$$

Furthermore, from (3.69) we easily find

$$\beta_{\pm}(t) = \pm \left[\alpha_+(t) - \alpha_-(t) \right]^{-1} \left[f H f - f(\alpha_{\mp} + n) \right] \quad (3.73)$$

and using (3.72) we have a solution for the residues.

There are a couple of interesting aspects to this solution. First, notice that since $H \sim |t|^{-1}$, $\alpha_{\pm}(t) \rightarrow -n$ as $|t|$ gets large. This, of course, is necessary to reproduce the Born terms. Second, if by chance we are dealing with a situation where the Born term factorizes, that is, if

$$f_{11}f_{22} - f_{12}^2 = 0 \Rightarrow \text{Det}[f] = 0$$

then one of the trajectories decouples from the system. In the notation of (3.72) and (3.73) it is the $(-)$ trajectory that decouples. Solving for $\alpha_+(t)$ in this case and using (3.73), we find

$$\beta_-(t) = \frac{-1}{\text{Tr}[fH]} \left[f H f - f \text{Tr}[fH] \right]$$

where we have used $\text{Det}[AB] = \text{Det}[A]\text{Det}[B]$. Using the fact that H is a diagonal matrix, we easily find that if $\text{Det}[f] = 0$, then all the elements of $\beta_-(t) = 0$, and so this trajectory decouples from the system. We see then that it is the simultaneous requirements of factorization in the Regge residues and nonfactorization in the Born terms that forces us to have more than one trajectory.

In the present problem of two coupled particles, we have used the first two terms in $\ln(-u)$ to determine the trajectories and residues of the two leading trajectories to this order in the couplings. As we continue the iteration scheme in this example it will not be necessary to introduce more trajectories with $\alpha \rightarrow -n$. I have explicitly verified that this is true in the $\ln^2(-u)$ term. Of course, when we include terms which are of higher order in the couplings, they change

the expressions for α_{\pm} and β_{\pm} just as they did in the single channel case discussed in the last section.

Suppose now that we want to treat a coupled channel problem with three particles and one type of Born term. In that case, we would use a 3×3 matrix to describe the scattering amplitudes, and it would, in general, be necessary to introduce three trajectories. The total number of unknowns in that case would be 30: three residue functions each of which is a 3×3 matrix, and 3 scalar trajectories. However, since we require each residue to be a symmetric matrix, there are really only 21 unknowns. In addition, each residue function has three factorization conditions associated with it, which further reduces the number of unknowns to 12. Now, we also require the amplitudes $\mathcal{M}_j^{\alpha\beta}$ to be symmetric matrices. That means that although each amplitude \mathcal{M}_j represents nine equations, only six of them are independent. Therefore, even in the case of three coupled particles all the required trajectories once again appear as distinct entities by the first iteration. This is easily seen to be a general feature of our system and applies to cases with any number of particles (including one). Of course, it may happen that some trajectories accidentally coincide even after the first iteration. In that case, higher order terms are required to separate them, but this is a situation familiar from degenerate perturbation theory in nonrelativistic quantum mechanics. In fact, this entire discussion is quite reminiscent of many problems encountered there, for instance the Zeeman splitting of energy levels in a weak magnetic field.

An amusing way to see why two Regge trajectories are natural in a two particle coupled channel problem is to consider the following (classical) problem. Suppose I have a chain with $N+1$ links. The links can be of two types, A and B. The probability that at a given junction the two adjacent links will be of different

types is P . If the first link in the chain is of type A, what is the probability that the last link will also be of type A? We want to know, therefore, the probability that the links will change types an even number of times. The probability that they will change ℓ times regardless of order is

$$\frac{N!}{\ell! (N-\ell)!} P^\ell (1-P)^{N-\ell}.$$

To get our answer, we want to sum over even values of ℓ from zero to N . This is equivalent to performing the following sum over all ℓ :

$$\begin{aligned} & \frac{1}{2} \sum_{\ell=0}^N \frac{N!}{\ell! (N-\ell)!} \left[P^\ell (1-P)^{N-\ell} + (-P)^\ell (1-P)^{N-\ell} \right] \\ &= \frac{1}{2} \left[1 + (1-2P)^N \right] \end{aligned}$$

Now, suppose the probability of having a chain with $N+2$ links is proportional to

$$\frac{g}{(-u)^n} \frac{g^N \ell^n (-u)^N}{N!},$$

as in our case. (The Born term has two links and one junction.) Then, the total probability of having a link of type A at the far end of the chain if there is such a link at the near end, regardless of the number of links is

$$\begin{aligned} & \sum_{N=0}^{\infty} \frac{g}{(-u)^n} \frac{g^N \ell^n (-u)^N}{N!} \frac{1}{2} \left[1 + (1-2P)^{N+1} \right] \\ &= \frac{1}{2} g(-u)^{g-n} + \frac{1}{2} g(1-2P)(-u)^{g(1-2P)-n} \end{aligned} \quad (3.74)$$

and we see the emergence of two terms which look like Regge trajectories.

Notice that the second trajectory decouples if $P = \frac{1}{2}$, which in this example is the factorization condition for the Born term. Furthermore, if $P = \frac{1}{2}$, the

trajectory associated with the decoupled residue is independent of g and retains its asymptotic value of $-n$. This is exactly what happens in the two particle case we discussed earlier: from (3.72) we see that $\alpha_-(t) = -n$ if $\text{Det } f = 0$. This simple example, then, clearly illustrates the basic structure of the coupled channel equations.

Let us now turn to the more general problem in which the Born terms do not all have the same power fall-off in $|u|$. There are several new features to consider here. First, we will want to see how the trajectories whose asymptotic limit is $-n$ contribute to processes whose Born term $\propto (-u)^{-m}$. It is especially important to consider such contributions in the deep region when $m > n$. Second, we must examine the nature of the cross terms in the iteration scheme and see how they modify the deep scattering behavior of the amplitudes.

A problem of sufficient complexity to illustrate these points is the example of the coupled $k^+ - p$ system described above. Let us consider, then, the contributions of the first iteration to the $p-p$ elastic amplitude. With the choice of Born elements that are zero given below (3.64), we find that no cross terms $\propto f h$ contribute to \mathcal{M}^{22} in this order. Adding the two diagonal terms which contribute to \mathcal{M}_1^{22} to the $p-p$ Born term, we find that as far as its dependence on t and u are concerned, \mathcal{M}^{22} has the following asymptotic form to this order:

$$\mathcal{M}^{22} \sim \frac{h^{22}(t)}{(-u)^m} \left[1 + \frac{h^{22}(t)}{(-t)} \ln(-u) \right] + \frac{[f^{12}(t)]^2 \ln(-u)}{(-t)(-u)^n} . \quad (3.75)$$

where we have used the fact that $H(t) \sim (-t)^{-1}$ for large $|t|$. (We have not kept track of the numerical factors in $H(t)$ in (3.75), but they are of no consequence for this discussion.) In the first term we see the beginning of the Regge trajectory which goes to $-m$ at large $|t|$. Notice that there is only one trajectory here since in the present example there is only one non-zero element in the matrix h .

To understand the second term, we refer to (3.73). Remembering that $f^{22}=0$, the second term in the numerator is seen to be zero in the expression for β_{\pm}^{22} , and we have (asymptotically)

$$\beta_{+}^{22}(t) = -\beta_{-}^{22}(t) = \left[\alpha_{+}(t) - \alpha_{-}(t) \right]^{-1} (-t)^{-1} \left[f^{12}(t) \right]^2.$$

Therefore, the second term on the right of (3.75) may be expressed asymptotically as,

$$\begin{aligned} \beta_{+}^{22}(-u)^{\alpha_{+}} + \beta_{-}^{22}(-u)^{\alpha_{-}} &\approx (-u)^{-n} \beta_{+}^{22} \left[1 + (\alpha_{+} + n) \ln(-u) - 1 - (\alpha_{-} + n) \ln(-u) \right] \\ &= \frac{\left[f^{12}(t) \right]^2 \ln(-u)}{(-t)(-u)^n} \end{aligned}$$

as advertised in (3.75). The terms proportional to $\ln^0(-u)$ in the expansions of the two trajectories which approach $-n$ therefore cancel in the amplitude \mathcal{M}^{22} . This cancellation can be traced to the vanishing of the second term in the numerator of (3.73) for β_{\pm}^{22} , and is therefore due to the fact that $f^{22} = 0$.

Another interesting aspect of (3.75) is that it indicates the existence of a consistency condition on our theory. Since the Born terms are, by definition, those terms which dominate in the deep region, all the terms generated in \mathcal{M}_1^{22} , must be smaller than \mathcal{M}_0^{22} in this region. In the last section we used this criterion to define the onset of the deep region. However, one's intuition would certainly consider large fixed angles and $|u| \rightarrow \infty$ as sufficient criteria for at

least part of the deep region. Suppose that for large $|t|$ $f^{12}(t) \sim (-t)^{-A}$, $h^{22}(t) \sim (-t)^{-B}$. Then, for the Born term to dominate (3.75) in this region we require

$$B + m < 2A + n + 1. \quad (3.76)$$

Stated somewhat more clearly, the situation is this: suppose you give me a set of amplitudes which you claim describe large angle, high energy scattering. If your theory allows me to iterate these amplitudes in the t-channel and if your large angle scattering amplitudes do not satisfy a condition like (3.76), then your theory is probably inconsistent. Of course, this reasoning does not apply to theories that do not allow t-channel iterations, for example, a field theory in which deep scattering is described by an infinite t-channel sum of some irreducible kernel. In that case, t-channel iterations of the deep amplitude would introduce double counting of graphs and would not be allowed. In the parton interchange theory, a two channel system involving particles whose electromagnetic form factors behave differently at large $(-q^2)$ always gives Born matrices which have a structure like that described below (3.64) for the $k^+ - p$ system. If the form factors of the two particles fall off asymptotically as $(-q^2)^{-C}$ and $(-q^2)^{-D}$ with $C > D$, the consistency condition (3.76) becomes

$$D < C < 2D + 1 \quad (3.77)$$

If the k^+ form factor is a monopole and the nucleon form factor a dipole, this condition is satisfied. However, (3.77) could easily be violated if one attempted to describe the deep scattering of particles which have $D \lesssim 0.5$ and/or $C \gtrsim 2.5$; then somebody would be in trouble. The most reasonable conclusion in that case is simply that constituent interchange does not describe the deep scattering of such systems. Inequalities similar to (3.76) can also be extracted from higher

order matrix elements, but in general they will be less tight because of the accumulation of factors of $(-t)^{-1}$ from the H matrix.

Let us now briefly examine how the cross terms affect the amplitudes in the coupled channel case. In the present example, there will be cross terms contributing in second order to the transition amplitude, \mathcal{M}^{12} . On the basis of the previous discussions in this section, we easily find that to second order in the couplings the transition amplitude has terms of the form (mod constant factors, as in (3.75))

$$\mathcal{M}^{12} \sim \frac{f^{12}}{(-u)^n} \left[1 + \frac{f^{12} \ln(-u)}{(-t)} \right] + \frac{f^{12} h^{22}}{(-t)(-u)^n} + \frac{f^{12} h^{22}}{(-t)(-u)^m} \quad (3.78)$$

All the terms generated by \mathcal{M}_1^{12} , except the last, are obviously smaller than the Born term in the fixed angle region. For this to be true also for the last term, we require

$$n < m + B + 1 \quad (3.79)$$

with B defined above (3.76). It is noteworthy that this is automatically satisfied in the parton interchange theory, since in order to get Born matrices with the appropriate zero elements it is necessary that $m > n$. Finally, we note that the second term in (3.78) is $(-u)^{-n}$ times a second order contribution to the residues which couple the trajectories that asymptotically approach $(-n)$ to the transition amplitude. Similarly, the last term displays the lowest order contribution to the residues which couples the trajectory that goes to $(-m)$ as $|t|$ gets large with the transition amplitude, \mathcal{M}^{12} .

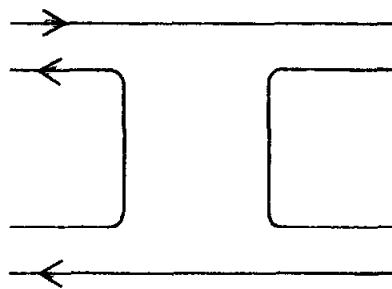
We have tried in this section to illustrate some of the new features which arise in the Reggeization of coupled channel problems. In general, it is clear

that in a problem with N particles, the number of trajectories generated is NM where M is the number of distinct types of Born terms. Of course, some of these trajectories may decouple from the system if some of the Born terms satisfy factorization. In what we have done so far, we have allowed Born amplitudes and kernels which have only right hand discontinuities in u . These generate purely real s -channel amplitudes. In the next section, we want to generalize these considerations to include sub-amplitudes with left hand discontinuities in u so that we can build up the imaginary parts of the scattering amplitudes required by s -channel unitarity as well as high energy phenomenology.

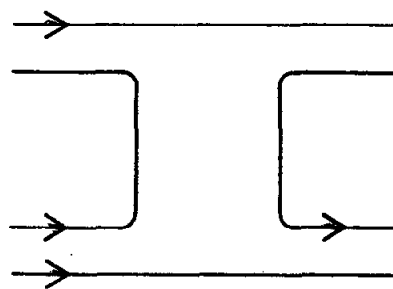
D. Signature, Duality Diagrams, and the Pomeron

All the results which we have derived so far in this chapter have assumed that the Born term and kernel (and therefore the amplitudes built up by t -channel iteration) have had singularities in u only for positive u . In general, of course, this is an unrealistic assumption when dealing with high energy scattering processes. In this section, we wish to remedy this situation, and enlarge our formalism to include singularities for $u < 0$ ($s > 0$). In doing so, we shall develop all the tools necessary in order to correctly include signature factors in Regge trajectories. We will also gain some insight into the nature of exchange degeneracy and the Pomeron pole, and we will discuss a possible relationship between the quarks used in the parton interchange theory²¹ (current quarks) and the quarks used in the Harari-Rosner duality diagrams.³⁰ A specific, realistic example of coupled $2 \rightarrow 2$ hadron-hadron amplitudes using the ideas developed in this section will be discussed in detail elsewhere.³¹

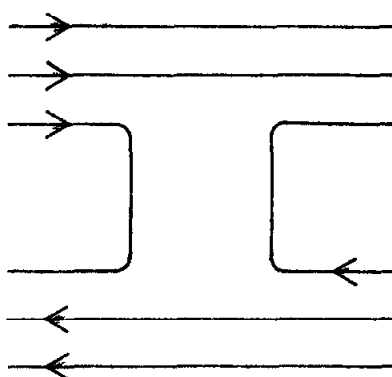
Before deriving the results we need, it is useful to review the basic properties of duality diagrams³⁰ as well as some aspects of the interchange theory.²¹ To begin, let us turn to Fig. (22), where we exhibit some duality diagrams for



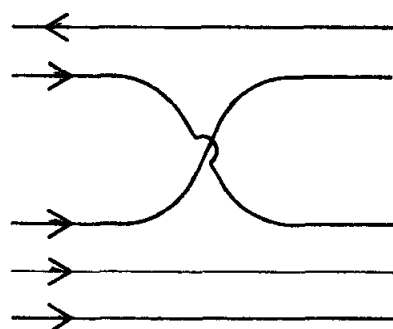
(a)



(b)



(c)



(d)

2319A22

FIG. 22--Some examples of the Harari-Rosner duality diagrams.

meson-meson, meson-baryon and baryon-antibaryon scattering. The external mesons are composed of quark-antiquark, and the external baryons (antibaryons) are composed of 3 quarks (antiquarks). These combinations are termed "non-exotic". This implies that the non-exotic mesons must belong to the 1 or 8 representations of SU(3), while the baryons must belong to the 1, 8 or 10 representations. Any other combinations of quarks and antiquarks are termed "exotic". Notice that this means, for example, that a particle constructed from $qq\bar{q}$ is exotic even though it belongs, say, to an SU(3) octet. The same rules of exoticity apply to the intermediate states in the duality diagrams. Therefore, for instance, both the s and t channels of Fig. (22b) are non-exotic, but only the t-channel of Fig. (22c) is non-exotic.

The duality diagrams are generally interpreted in the spirit of two component duality as applying only to the non-pomeron part of the amplitude. A diagram which is planar and non-exotic in two channels is taken as a graphical representation of the Regge-resonance duality between those two channels. More specifically, the rules for drawing the Harari-Rosner duality diagrams are:

- (i) Quarks do not change their identity in the graph and are represented by continuous lines.
- (ii) External baryons (qqq) are represented by three lines running in the same direction, and external mesons ($q\bar{q}$) are represented by two lines running in opposite directions.
- (iii) Both ends of a single line cannot belong to the same external particle.

A "legal" duality diagram also obeys the rule

- (iv) Any $B = \pm 1$ intermediate state (B in Baryon number) can be cut by slicing through only three lines, and any $B = 0$ intermediate state can be cut by slicing through two lines.

There seems to be no obvious problem with these rules for $M\text{-}M$ and $M\text{-}\bar{B}$ scattering, since, in general, we can draw legal, planar diagrams for non-exotic reactions as in Figs. (22a and b). For $B\text{-}B$ scattering, we do not expect to be able to draw legal diagrams with non-exotic intermediate states since $B = 2$ is exotic. We run into trouble, however, with $B - \bar{B}$ scattering, Fig (22c). Here, the s and t channels may not have exotic quantum numbers, but there seems to be no way to draw a legal diagram for this process which has non-exotic quantum numbers in both channels. This would appear to indicate the existence of important exotic contributions to the imaginary part of the scattering amplitude, contrary to the first order assumption of absence of exotics and EXD (exchange degeneracy). We shall not directly deal with the $B\text{-}\bar{B}$ problem here, but the interested reader can refer to the literature for extensive discussions.³²

The duality property of the diagrams which are planar and non-exotic in two channels is, like most duality arguments, applicable only to the imaginary part of the amplitude. In Fig. (22d), we have drawn a diagram which is planar and non-exotic in the u and t channels. This represents the duality between the u -channel resonances and t -channel exchange contributions to the imaginary part of the amplitude at large u and small $|t|$, but according to our rules is not a legal diagram in the $s\text{-}t$ plane. This means that it does not represent any contributions to the imaginary part of the amplitude at large s and small $|t|$. We therefore expect this diagram to be real at large s and small $|t|$. Furthermore, it is a useful observation that $s\text{-}t$ and $u\text{-}t$ diagrams are the most important diagrams for forward elastic scattering, while $u\text{-}t$ and $s\text{-}u$ diagrams are most important for backward elastic scattering.

The correlation of the inability to draw a legal, planar duality diagram with a vanishing non-diffractive imaginary part leads very simply to many predictions.

For instance, $k^+ n \rightarrow k^0 p$ and $k^- p \rightarrow \rho^0 \Lambda$ are predicted to be purely real at small $|t|$. $k^+ p \rightarrow k^+ p$, on the other hand has an imaginary part near $t = 0$, but this is supposed to come from Pomeron exchange. The imaginary parts of the ordinary Regge exchanges are predicted to cancel in this reaction. Many more similar prediction may be found in Refs. 30.

The reader has undoubtedly noticed that we have been qualitatively discussing duality diagrams, but have not described any specific calculational scheme associated with them. The interpretation of duality diagrams is not unambiguous, and so it is not clear how to calculate them. This ambiguity is illustrated by the fact that the two authors who independently introduced duality diagrams take different approaches to them.³⁰ Harari does not present any rules of calculation for the diagrams, while Rosner does. In Rosner's scheme, one adopts a Regge description for the amplitude with factorizable residues. The couplings are then calculated by taking SU(3) traces, and duality conditions become constraints on trajectories and couplings. While this scheme involves more assumptions than the approach taken by Harari, it should yield a wider class of predictions. However, for our purposes, it is appropriate to adopt Harari's philosophy, and consider duality diagrams as a simple visual mnemonic for keeping track of quarks.

Before leaving this topic, we want to emphasize what is, for us, the most important aspect of duality diagrams. If you can't draw a planar (st) duality diagram for a $2 \rightarrow 2$ hadronic amplitude, the normal Regge poles, excluding the Pomeron, which contribute to high energy, small $|t|$ scattering are predicted to be exchange degenerate.

Now let us briefly review the parton interchange theory of deep hadron-hadron scattering.²¹ In this theory, deep scattering is supposed to take place

by the interchange of constituents of the scattering hadrons. No direct scattering between constituents is required. Only the "simplest" part of the hadrons' wave functions are supposed to be important in the deep region, and this part is taken to be the amplitude for finding the smallest possible number of constituents in the hadron. These constituents are assumed to carry quark quantum numbers. More specifically, the interchange picture assumes a wave function for a hadron to be a quark and a "core", the core representing the collective effects of the other constituents. A typical interchange diagram is shown in Fig. (15). The heavy lines are hadrons, the jagged lines are cores, and the light internal lines are quarks. The blobs at the vertices represent the wave function for finding the hadron in the state represented by the internal lines. This diagram happens to be a (tu) graph, since it is planar in the t and u channels. To get the complete amplitude, one must add together all allowed interchange diagrams. There are only a few such diagrams, however, since it is assumed that the amplitude for a hadron to be a quark and a core in this kinematic region is non-negligible only if the quark happens to be of a type given by the naive quark model. (Actually, these are current, rather than constituent quarks, but the statement about quark type is still correct.)

The similarity between Fig. (15) and Fig. (22d) is clear. The exchanged objects in the two figures are not a priori the same, but the topologies of the graphs are the same. This is a general feature of the interchange theory — the topologies of the contributing interchange graphs for deep scattering are the same as the topologies of the duality diagrams which one can draw for the given reaction (according to the rules given on p. 99), and which are supposed to describe the non-diffractive part of the scattering in the Regge region. After we develop the tools we need, we will return to the question of the relationship between these two sets of diagrams.

To develop these tools, we turn now to the problem of generalizing our recursion relations, (3.19a) or (3.19b), to cases where the kernel or the Born term has discontinuities in u for $u < 0$ — or more exactly, where there are singularities in s for $s > 0$. In the context of the interchange theory, (st) graphs like Fig. (23) have singularities in s for $s > 0$, but no singularities in u for $u > 0$, while (su) graphs as shown in Fig. (24) have singularities both for $s > 0$ and $u > 0$. Of course, any theory of deep scattering may have terms with these singularities, so in general, it is important to consider this problem. Naturally, our results are not limited to the parton-interchange model, but are as general as our original recursion relations (3.19a) and (3.19b) are.

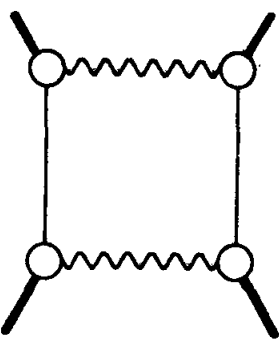
Let us first consider convoluting an amplitude, \mathcal{M}_j , which has only u -channel discontinuities ($u > 0$) with a kernel which has only s -channel singularities. Using the frame and parameterization of (3.14) and the labelings shown in Fig. (11), we can introduce a dispersion relation for K in the variable $s' = (p+q)^2$, which is the s of the subamplitude, K . We can write

$$K(s', t; N^2, \Lambda^2) = \int d\sigma^2 \frac{W(\sigma^2, t; N^2, \Lambda^2)}{(p+q)^2 - \sigma^2 + i\epsilon} . \quad (3.80)$$

Of course, the comments we made in section B about the path of integration in the complex σ^2 -plane and the Λ^2 -dependence of K apply here also.

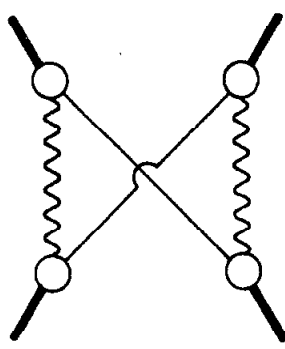
Using (3.15) and (3.80) in (3.10), we have

$$\begin{aligned} \mathcal{M}_{j+1} = & \frac{1}{2(2\pi)^4} \int_{-\infty}^{\infty} \frac{dy d^2 \ell_1 d\ell^2}{2|y|} d\sigma^2 d\rho^2 \left[\ell^2 - M^2 + i\epsilon \right]^{-1} \left[(\ell+q)^2 - M^2 + i\epsilon \right]^{-1} \\ & \left[(\ell-r)^2 - \rho^2 + i\epsilon \right]^{-1} \left[(p+\ell+q)^2 - \sigma^2 + i\epsilon \right]^{-1} W_j(\rho^2) W(\sigma^2) \end{aligned} \quad (3.81)$$



2319A23

FIG. 23--(st) parton-interchange graph.



2319A24

FIG. 24--(su) parton-interchange graph.

where we have used the transformation below (3.15), and have suppressed unimportant dependences in the arguments of \mathcal{M}_{j+1} and the W 's. As before, we now wish to perform the $d\ell^2$ integration. Using (3.14), we find after some algebra that if $1 + \frac{1}{y} > 0$, all four propagators have poles in the lower half ℓ^2 -plane and so we can close the $d\ell^2$ contour in the upper-half plane and we get zero. If, however, $1 + \frac{1}{y} < 0 \iff -1 < y < 0$, then the propagator from the dispersion relation (3.80) has its pole in the upper-half ℓ^2 -plane. Closing the contour around this pole (3.81) becomes,

$$\mathcal{M}_{j+1} = \frac{1}{2(2\pi)^3} \int_0^1 \frac{dx d\sigma^2 d\rho^2 d^2 \ell_\perp}{(1-x)x^3} \left[\nu^2 - S(\ell_\perp + q_\perp, x) \right]^{-1} \left[\nu'^2 - S(\ell_\perp + xq_\perp, x) \right]^{-1} \\ \left[s - S'(\ell_\perp + xq_\perp - (1-x)r_\perp, x) \right]^{-1} W_j(\rho^2) W(\sigma^2) \quad (3.82)$$

where we have set $x = -y$. S is defined in (3.17), and S' is defined below (3.18).

Now, since $d^2 \ell_\perp$ is integrated over the entire plane, we can shift $\ell_\perp \rightarrow \ell_\perp - xq_\perp$.

Doing this and redefining $x \equiv y$, and we can rewrite (3.82) as

$$\mathcal{M}_{j+1}(s, t; N^2, R^2) = \frac{1}{2(2\pi)^3} \int d\sigma^2 d\rho^2 \int_0^1 \frac{dy d^2 \ell_\perp}{y^3 (1-y)} \left[\nu'^2 - S(\ell_\perp, y) \right]^{-1} \\ \left[\nu^2 - S(\ell_\perp + (1-y)q_\perp, y) \right]^{-1} \left[s - S'(\ell_\perp - (1-y)r_\perp, y) \right]^{-1} W(\sigma^2, t; N^2, \Lambda^2) W_j(\rho^2, t; \Lambda^2, R^2) \quad (3.83)$$

Comparing (3.83) with (3.18), we see that they are the same with the substitutions $u \rightarrow s$, $\nu^2 \rightarrow \nu'^2$. In terms of momenta this is just the well-known substitution formula for s - u crossing: $p \rightarrow -(p+q)$. Therefore \mathcal{M}_{j+1} in (3.83) is gotten from \mathcal{M}_{j+1} in (3.18) by $s \leftrightarrow u$ crossing.

It is easy to understand this result by considering an example in which the sub-amplitudes are simple poles in the appropriate variable. In Fig. (25a), we show the kernel with a simple pole at positive u , while (25b) shows the kernel with a pole for positive s . The arrows on the lines indicate which particles are entering and which are leaving the graph. We form an amplitude composed of two u -channel poles as in Fig. (26a) by simply joining two terms of type (25a) to each other. Similarly in Fig. (26b) we illustrate the result of combining an amplitude like (25b) with an amplitude like (25a). The topology is, of course, dictated by the fact that we must join lines together so that the quantum number and momentum flow is continuous. The equality in Fig. (26b) follows by simply redrawing the graph and switching the positions of the top two vertices. We now clearly see that (26b) is related to (26a) by $s \leftrightarrow u$ crossing, and so we can understand the result (3.83).

For our purposes it is convenient to categorize amplitudes according to whether they have discontinuities for positive u or positive s . Such amplitudes will be referred to as u amplitudes and s amplitudes, respectively. Amplitudes possessing singularities both for positive s and positive u will be called su amplitudes. (In another language, these are the graphs with non-zero Mandelstam third double spectral functions.) For example, the (ut) parton interchange graph of Fig. (15) is a u amplitude, while Fig. (23) is an s amplitude and Fig. (24) an su amplitude.

On the basis of the discussion in section B, and (3.83), we can construct the following rules which express the topology of amplitudes obtained by

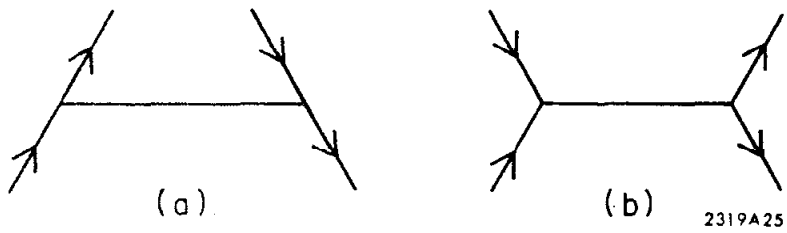
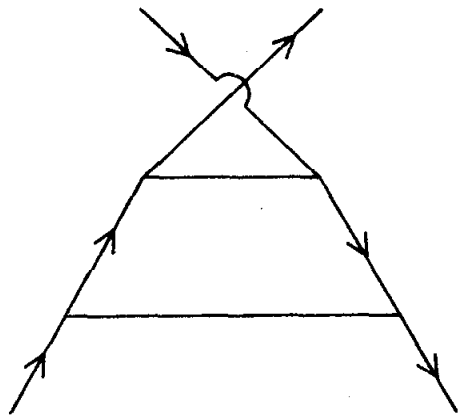
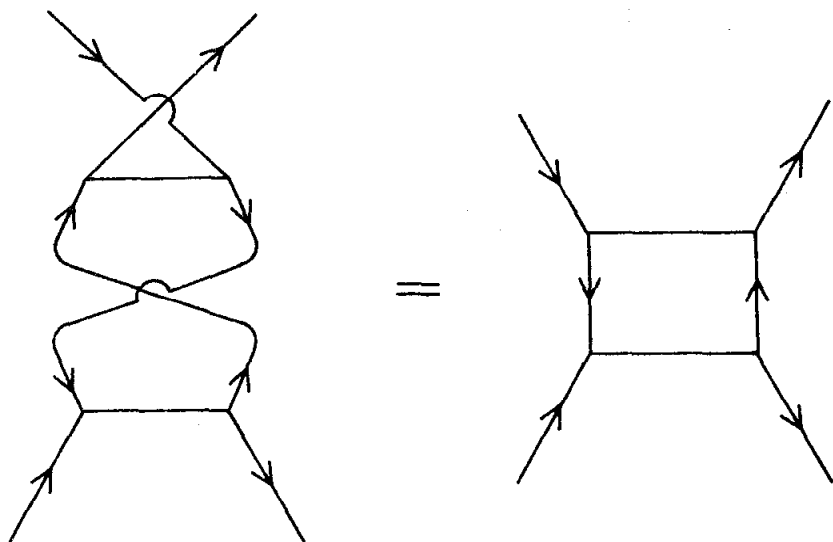


FIG. 25--Simple amplitudes with (a) u-channel and (b) s-channel singularities (in this case poles).



(a)



(b)

2319A26

FIG. 26--Feynman diagrams resulting from the convolution of subamplitudes as in Fig. 25; (a) is the result of $u \times u$ and (b) is the result of $s \times u$.

convoluting various sub-amplitudes in our iteration scheme:

$$\begin{aligned}
 u \times u &= u \\
 s \times u &= s \\
 u \times s &= s \\
 s \times s &= u
 \end{aligned} \tag{3.84}$$

The first equation in (3.84) follows from the discussion of section B, and the second is the result expressed in (3.83). The last two can be proved by deriving appropriate formulae similar to (3.83), or the reader may simply convince himself of their correctness by drawing diagrams as in Fig. (26).

We now must discuss how to handle sub-amplitudes with non-zero third double spectral functions — the su amplitudes. We will briefly describe the method for coping with such graphs here. Suppose, then, that we wish to use an su amplitude for the lower blob in, say, Fig. (11). An example of such an insertion is the parton-interchange (su) diagram of Fig. (24). Such a graph has singularities for both positive s and positive u . It is convenient to introduce a double dispersion relation for this kind of amplitude:

$$K(s, u) = \int \frac{d\sigma^2 d\tau^2 W(\sigma^2, \tau^2)}{[s - \sigma^2 + i\epsilon] [u - \tau^2 + i\epsilon]} . \tag{3.85}$$

If, for instance,

$$K = (\mu^2 - u)^{-n} (\mu^2 - s)^{-m}$$

then

$$W = \frac{\delta^{[n-1]} (\mu^2 - \tau^2)^{[n-1]} \delta^{[m-1]} (\mu^2 - \sigma^2)^{[m-1]}}{(n-1)! (m-1)!} .$$

Inserting this expression in our convolution formula, for example, (3.10) we have

$$\mathcal{M}_{j+1} = \int \frac{d^4 \ell}{(2\pi)^4} d\sigma^2 d\tau^2 \left[\ell^2 - M^2 + i\epsilon \right]^{-1} \left[(\ell+q)^2 - M^2 + i\epsilon \right] \left[(p+\ell+q)^2 - \sigma^2 + i\epsilon \right]^{-1} \left[(p-\ell)^2 - \tau^2 + i\epsilon \right]^{-1} W(\sigma^2, \tau^2) \mathcal{M}_j \quad (3.86)$$

where the u and s of the kernel are $u' = (p-\ell)^2$ and $s' = (p+\ell+q)^2$. On the basis of the discussions in this section and section B, we note the following: when we do the $d\ell^2$ integration (after performing the transformation following (3.15)), we find that there are two contributions to \mathcal{M}_{j+1} . The pole from the propagator $[(p+\ell+q)^2 - \sigma^2 + i\epsilon]^{-1}$ is the only singularity in the upper half ℓ^2 -plane for $-1 < y < 0$, while for $0 < y < 1$, the pole from the propagator $[(p-\ell)^2 - \tau^2 + i\epsilon]^{-1}$ is the only one in the upper-half plane. Hence, after doing the $d\ell^2$ integral there are two pieces that add together to make up \mathcal{M}_{j+1} . The first, coming from the region $-1 < y < 0$ has the same topological character as if we had used only an s amplitude for the kernel, while the second ($0 < y < 1$) behaves as if the kernel were a u amplitude. Therefore, for the purposes of our convolution scheme, the su amplitude can be considered to be the sum of an s plus a u amplitude, or symbolically,

$$\begin{aligned} su \times u &= s \times u + u \times u = s + u \\ su \times s &= s \times s + u \times s = u + s \\ su \times su &= s \times s + s \times u + u \times s + u \times u = s + u. \end{aligned} \quad (3.87)$$

Naturally, the coefficients of the various contributions depend on the specific case, but their topological character is represented in (3.87).

In order to gain some insight into the significance of the topology of the amplitudes (as expressed in the rules (3.84) and (3.87)), let us compare two simple examples of ladder graphs. In both examples, we use a perturbation approximation, keeping the minimum possible factors of the coupling constant, g to each order in $\ln s$ (or $\ln u$). First, suppose that the kernel and Born term are simple u -channel poles. For small g , the j^{th} iteration of this pole has a leading contribution

$$\mathcal{M}_j \sim \frac{g}{(-u)} \frac{g^j \ln^j(-u)}{j!}$$

Summing one n , we have

$$\mathcal{M} = \sum_{j=0}^{\infty} \mathcal{M}_j \sim g (-u)^{g-1} .$$

We have neglected the t -dependence here since it is not important for this argument.

This is a special case of (3.40) for simple ladders (neglecting t -dependence), and will be recognized, as we have emphasized before, as a sum of exchange degenerate trajectories:

$$g(-u)^{g-1} = \frac{g}{2} \left[(-u)^{g-1} + (-s)^{g-1} \right] + \frac{g}{2} \left[(-u)^{g-1} - (-s)^{g-1} \right] \quad (3.88)$$

This strong exchange degeneracy is, of course, due to the fact that the convolution of two u amplitudes always gives a u amplitude (see (3.84)).

Now consider a case in which we again iterate simple poles, but this time the poles are s -channel poles; i.e., the Born term and kernel is

$$K = \frac{g}{\frac{2}{\mu} - s + i\epsilon} .$$

Following the previous discussion of this section, working in a perturbation approximation, and neglecting t -dependences, we find that the leading contribution to the j^{th} iteration is

$$\mathcal{M}_j \sim \begin{cases} \frac{g}{(-s)} \frac{g^j \ln^j(-s)}{j!} ; & j \text{ even} \\ \frac{g}{(-u)} \frac{g^j \ln^j(-u)}{j!} ; & j \text{ odd} \end{cases}$$

This behavior is also given by the equations (3.84). We can sum \mathcal{M}_j over j to get the full amplitude as follows:

$$\begin{aligned} \mathcal{M} = \sum_{j=0}^{\infty} \mathcal{M}_j &= \sum_{j, \text{ even}} \frac{g}{(-s)} \frac{g^j \ln^j(-s)}{j!} + \sum_{j, \text{ odd}} \frac{g}{(-u)} \frac{g^j \ln^j(-u)}{j!} \\ &= \frac{g}{2(-s)} \left\{ \sum_j \frac{g^j \ln^j(-s)}{j!} + \sum_j \frac{(-g)^j \ln^j(-s)}{j!} \right\} \\ &+ \frac{g}{2(-u)} \left\{ \sum_j \frac{g^j \ln^j(-u)}{j!} - \sum_j \frac{(-g)^j \ln^j(-u)}{j!} \right\} \\ &= \frac{g}{2} \left\{ (-s)^{g-1} + (-s)^{-g-1} + (-u)^{g-1} - (-u)^{-g-1} \right\} \\ &= \frac{g}{2} \left[(-u)^{g-1} + (-s)^{g-1} \right] - \frac{g}{2} \left[(-u)^{-g-1} - (-s)^{-g-1} \right] \end{aligned} \quad (3.89)$$

This amplitude is therefore given by a sum of two non-exchange degenerate Regge poles, one of positive signature and one of negative signature. In the simple case we have been considering, the two trajectories are displaced from each other by an amount $2g$ (at $t = 0$). Of course, this is only because we have ignored many of the features which are important in a realistic case, and the

exact dependence of the trajectories on t is much more complicated. Nonetheless, the basic feature of (3.89), namely, the lack of exchange degeneracy, will clearly be unaffected by these complications.

What is the significance of this in view of the parton interchange theory? In this theory, the (tu) graphs (Fig. (15)) have the topology associated with u amplitudes while the (st) graphs (Fig. (23)) are like s amplitudes. In a world with only one kind of sub-amplitude, the character of the full amplitude, \mathcal{M} , is the same as the character of the Born term. A (tu) Born term gives rise to a pair of exchange degenerate Regge trajectories, while an (st) Born term generates non-exchange degenerate poles. Duality diagrams, on the other hand, tell us whether in the Regge region the non-diffractive Regge poles are exchange degenerate, or not. With a given pair of initial state particles, the topology of the Born term and duality diagram is the same, and so we have a simple one-to-one correspondence between the predictions of duality diagrams, and the predictions of our iteration scheme.

While it is interesting to see the close relationship between the topology of the Born term and the duality diagram in these simple, single channel cases, the real hadronic world is significantly more complicated. The most glaring shortcoming of the single channel case is that we evidently do not generate anything that corresponds to a Pomeron pole since a single channel treatment of, for example, proton-proton elastic scattering gives a purely real amplitude, even at $t = 0$. The way to cure this disease is to consider the more realistic coupled channel case.

Let us look for a moment at p - p elastic scattering. In the first iterated amplitude, the intermediate t -channel state may consist of a p - \bar{p} pair, but it may also be a π - $\bar{\pi}$ pair or a k - \bar{k} pair, etc. The p - \bar{p} state will only contribute a

real piece to the total amplitude, but many of the other intermediate states will generate imaginary parts. The way in which these different channels mix together to break the exact exchange degeneracy and to generate other poles is quite complicated, but we can gain some insight into the general nature of the process by the following considerations: as we approach the Regge region (say, fixed t , $|u| \rightarrow \infty$), our formulae show that the higher order iterations become more and more important. In the coupled channel case, this means that it is more and more likely that the original hadrons coming in at the bottom of the graph will forget what they are, since they have more chances of changing their identity. From the probability argument in section C, (above (3.74)), we see that for very large N , the probability that after N rungs the first link is of the same type as the last link $\rightarrow \frac{1}{2}$, regardless of the value of P . This indicates that in the kinematic region where large numbers of iterations are important (the Regge region), all the hadronic amplitudes will behave roughly the same. Qualitatively, this is what is expected from diffractive scattering. As $|u| \rightarrow \infty$, the graphs with more rungs become more important and the hadrons tend to forget what they were. Similarly, when $|u| \rightarrow \infty$, the Pomeron pole becomes more important relative to the non-diffractive trajectories. Therefore, we propose that the extent to which the Pomeron dominates the bulk of hadronic high energy scattering, is a rough measure of how much the original hadrons forgot what they were on their way up the t -channel ladder.

A few remarks are certainly in order about this discussion. First, the relationship we have outlined between parton-interchange diagrams and duality diagrams may be interpreted as a relationship between current quarks and duality diagram quarks. The duality diagram quarks really contain contributions not only from the current quarks appearing in the interchange Born terms, but

also contain contributions from the quarks which comprise the numerous t -channel intermediate states that contribute to the entire amplitude in the Regge region. Second, we cannot (at this point, anyhow) claim to have explained many of the interesting properties of the Pomeron, for instance the nature of its trajectory near $t = 0$. This is because a detailed determination of trajectories at small $|t|$ is, from this point of view extremely complicated. Third, even if we could calculate the Pomeron, that would not be the whole story, since for such a high lying pole ($\alpha(0) \approx 1$) j -plane cuts arising from the iteration of the pole in the s -channel may be important and are presumably not contained in the set of graphs which we calculate. Finally, for a completely consistent interpretation, we must also examine backward scattering, and show that the intermediate states are such that the leading trajectory is significantly different from the leading trajectory in the forward direction — in particular, that it is not the Pomeron.³³

Work on these points and speculations is in progress, and will be reported elsewhere.³¹

CHAPTER IV

SUMMARY AND CONCLUSIONS

In this work, we have examined some aspects of the deep hadron-hadron scattering region. To conclude, we briefly list the major results which have been obtained:

1. A simple and natural extension of the ideas of the Feynman parton model result in an asymptotic formula for the average multiplicities in inclusive or semi-inclusive hadron-hadron scattering experiments in which at least one particle is detected with a large transverse momentum. Furthermore, we have shown that it is possible to relate these multiplicities to the multiplicities observed in other high energy reactions, specifically $e^+ e^-$ annihilation, deep inelastic lepto-production, and ordinary (not associated with large transverse momenta) hadron-hadron collisions.

2. An integral equation for hadron-hadron scattering amplitudes is derived. The kernel for the equation is taken to be a (2-particle irreducible) deep scattering amplitude for a $2 \rightarrow 2$ hadron-hadron scattering process. The integral equation is then used to show how the deep scattering region is connected to the Regge region and how Regge poles are built up by t-channel iteration of the kernel.

3. A number of simple cases are analyzed with the help of a Mellin transform technique. A few examples of possible kernels for the integral equation are discussed. They help to show more clearly how the deep and Regge regions are connected, and what the important s-channel and t-channel intermediate states are in the two domains. The connection of our approach with Feynman's notions about wee partons is also elucidated.

4. Our equation is generalized to allow us to discuss coupled channel scattering problems, and a two-channel problem is described in detail. The Regge

trajectories generated by the t-channel iteration scheme turn out to be the eigenvalues of a matrix equation.

5. The integral equation is further generalized to include the effects of signature, since all the previous discussions were presented for amplitudes which are purely real. Simple rules are derived which express the phase of the amplitude obtained by tying two sub-amplitudes together in our iteration scheme.

6. We apply our Reggeization scheme to the parton-interchange model of deep scattering, and find an interesting correlation between parton-interchange diagrams and the Harari-Rosner duality diagrams. This correlation leads us to some interesting speculations on the nature and dynamical origin of the Pomeron pole.

Aside from this summary, the only appropriate comment to make here about deep hadron-hadron scattering is that although this kinematic domain has not yet been extensively studied, early indications are that such studies will give us a much deeper understanding of the nature of hadronic interactions than we have now.

REFERENCES

1. See for example the review by W.R. Frazer, et al., Rev. Mod. Phys. 44, 284 (1972).
2. M. Jacob, in Proceedings of the XVI International Conference on High Energy Physics, National Accelerator Laboratory, Batavia, Illinois (1972).
3. R.P. Feynman, Phys. Rev. Letters 23, 1415 (1969).
4. R.P. Feynman in High Energy Collisions, Third International Conference on High Energy Collisions, Stony Brook (Gordon and Breach, New York, 1969).
5. R.P. Feynman, Photon-Hadron Interactions (W.A. Benjamin, New York, 1972).
6. See, for example, M. Bander, Phys. Rev. D 6, 164 (1972).
7. M. Gronau, F. Ravndal and Y. Zarmi, Caltech preprint CALT-68-367 (1972).
8. R.N. Cahn, J. W. Cleymans and E.W. Colglazier, Phys. Letters, 43 B, 323 (1973). The discussion of lepto-production multiplicities follows closely the discussion presented here.
9. S.M. Berman, J.D. Bjorken and J.B. Kogut, Phys. Rev. D 4, 3388 (1971).
10. S.D. Drell and T.M. Yan, Ann. Phys. 66, 578 (1971) and references therein. This article also contains a discussion of the ideas of the Feynman parton model.
11. J.D. Bjorken, Phys. Rev. D 7, 282 (1973).
12. The discussion here is based on R. Savit, Phys. Rev. D 8, 274 (1973).
13. J.F. Gunion, S.J. Brodsky and R. Blankenbecler, Phys. Rev. D 8, 287 (1973), and references therein.

14. J.D. Bjorken, private communication. I am grateful to Dr. Bjorken for several illuminating discussions on these points.
15. J.D. Bjorken and J.B. Kogut, Stanford Linear Accelerator Center report no. SLAC-PUB-1213 (1973) have recently suggested a correspondence argument which implies that $C_h = C_{e^+e^-}$.
16. This kind of parameterization has been used in the literature many times before. See, for example, Refs. 17, 19 and 21 below.
17. J.D. Bjorken, J.B. Kogut and D.E. Soper, Phys. Rev. D3, 1382 (1971).
18. This rule requires some delicacy when applied to theories involving particles with spin. For an explanation of these complications, see J.B. Kogut and D.E. Soper, Phys. Rev. D1, 2901 (1970), as well as Ref. 17 above.
19. S.J. Chang and S.K. Ma, Phys. Rev. 180, 1506 (1969), and M. Schmidt, Stanford Linear Accelerator Center Report No., SLAC-PUB-1265.
20. R. Blankenbecler, M.L. Goldberger, S.W. MacDowell and S.B. Trieman, Phys. Rev. 123, 692 (1961).
21. R. Blankenbecler in Proceedings of the Canadian Institute of Particle Physics Summer School, McGill University, 1972, Ed. R. Henzi and B. Margolis, pp 3-75; J.F. Gunion, S.J. Brodsky and R. Blankenbecler, Ref. 13 above.
22. It is possible, however, that a stable approximation procedure for $\mathcal{M}(t)$ can be worked out on the basis of (3.21). Such a procedure might initially require B and K only over a small range of t, and might yield a reliable expression for \mathcal{M} over a much wider t-range.
23. See, for instance, M. Jacob, CERN Preprint No. TH.1639-CERN, and references therein, for a summary of the large transverse momentum results obtained thus far at the ISR.

24. See, for example, T.K. Gaisser, Phys. Rev. D 2, 1337 (1970); H. M. Fried and K. Raman, Phys. Rev. D 3, 269 (1971); H. M. Fried, B. Kirby and T.K. Gaisser, Brown University Preprint No. COO-3130TA-274-Rev.; S. M. Berman, J. D. Bjorken and J. B. Kogut, Phys. Rev. D 4, 3388 (1971); D. Amati, L. Caneschi and M. Testa, Phys. Letters 43 B, 186 (1973), and CERN Preprint No. TH.1644-CERN; as well as Reference 21 above.
25. I. S. Gradshteyn and I. M. Ryzhik, Table of Integrals, Series, and Products (Academic Press, New York, 1965), p. 318.
26. M. Abramowitz and I. A. Stegun, Handbook of Mathematical Functions (National Bureau of Standards, Washington, D.C., 1964) p. 255 f f.
27. R. P. Feynman, Phys. Rev. Letters, 23, 1415 (1969) and Photon-Hadron Interactions (W.A. Benjamin, New York, 1972).
28. R. Savit, unpublished calculation.
29. J. C. Polkinghorne in Proceedings of the Canadian Institute of Particle Physics Summer School, McGill University, 1972, Ed. R. Henzi and B. Margolis, pp. 397-432.
30. H. Harari, Phys. Rev. Letters 22, 562 (1969); J. L. Rosner, Phys. Rev. Letters 22, 689 (1969).
31. R. Blankenbecler, S. Brodsky, J. Gunion and R. Savit, Stanford Linear Accelerator Report No., SLAC-PUB-1294, to be published in Phys. Rev. D; R. Savit and R. Blankenbecler, in preparation.
32. In addition to Refs. 30, the reader may consult J. L. Rosner, Phys. Rev. Letters 21, 950 (1968); J. Mandula, J. Weyers and G. Zweig, Phys. Rev. Letters 23, 266 (1969); J. L. Rosner, C. Rebbi and R. Slansky, Phys. Rev. 188, 2367 (1969); P.G.O. Freund, R. Waltz, and J. L. Rosner, Nucl. Phys. B 13, 237 (1969); J. L. Rosner, Invited talk presented at the Eastern

Theoretical Physics Conference, Syracuse, New York, 1969; M. Kugler, Phys. Letters 32 B, 107 (1970), and Acta Physica Austriaca, Suppl. VII, 443 (1970); T. Buhl, D. Cline and R. Terrell, Nucl. Phys. B37, 421 (1972); R. Savit, contribution to Critical Review of Phenomenological Duality, Stanford Linear Accelerator Center, Sept. 1972, unpublished.

33. We note parenthetically that for backward meson-baryon scattering there is a legal duality diagram (with a $B = 1$ state in the s and u channels) which has no counterpart in the parton interchange theory. This is because of the way the baryons are treated — as effective 2 body, rather than 3 body states.